Space Science Reviews (2025) 221:123
https://doi.org/10.1007/s11214-025-01248-5

Fundamentals of Interior Modelling and Challenges in the Interpretation of Observed Rocky Exoplanets

Philipp Baumeister[1] · Francesca Miozzi[2] · Claire Marie Guimond[3] · Marie-Luise Steinmeyer[4] · Caroline Dorn[4] · Shun-Ichiro Karato[5] · Émeline Bolmont[6] · Alexandre Revol[6] · Alexander Thamm[1] · Lena Noack[1]

Received: 17 April 2025 / Accepted: 18 November 2025

Abstract

Most our knowledge about rocky exoplanets is based on their measure of mass and radius. These two parameters are routinely measured and are used to categorise different populations of observed exoplanets. They are also tightly linked to the planet's properties, in particular those of the interior. As such they offer the unique opportunity to interpret the observations and potentially infer the planet's chemistry and structure. Required for the interpretation are models of planetary interiors, calculated a priori, constrained using other available data, and based on the physiochemical properties of mineralogical phases. This article offers an overview of the current knowledge about exoplanet interiors, the fundamental aspects and tools for interior modelling and how to improve the contraints on the models, along with a discussion on the sources of uncertainty. The origin and fate of volatiles, and their role in planetary evolution is discussed. The chemistry and structure of planetary interiors have a pivotal role in the thermal evolution of planets and the development of large scale properties that might become observables with future space missions and ground-based surveys. As such, having reliable and well constrained interior models is of the utmost importance for the advancement of the field.

✉ P. Baumeister
philipp.baumeister@fu-berlin.de

✉ F. Miozzi
fmiozzi@carnegiescience.edu

1 Department of Earth Sciences, Freie Universität Berlin, Malteserstrasse 74-100, 12249 Berlin, Germany

2 Earth and Planets Laboratory, Carnegie Institution for Science, 5241 Broad Branch Road NW, 20015, Washington D.C., USA

3 Atmospheric, Oceanic, and Planetary Physics, Department of Physics, University of Oxford, Parks Rd, Oxford OX1 3PU, UK

4 Institute for Particle Physics and Astrophysics, ETH Zurich, Wolfgang-Pauli-Strasse 27, 8093 Zürich, Switzerland

5 Department of Earth and Planetary Sciences, Yale University, 210 Whitney Ave, New Haven, CT 06520, USA

6 Department of Astronomy, Geneva University, 51 Chemin Pegasi, Sauverny, 1290, Switzerland

Published online: 03 December 2025

1 Introduction

Nearly 6000 exoplanets have been detected so far,[1] and this number continues to grow steadily. Although a variety of techniques exist for exoplanet detection, almost all low-mass planets have been discovered via the transit method, using data from the Kepler (Borucki et al. 2010) and TESS missions (Ricker et al. 2015), and via the radial velocity (RV) method (e.g. Vogt et al. 1994; Mayor et al. 2011; Seifahrt et al. 2018; Pepe et al. 2021). The upcoming PLATO mission (Rauer et al. 2014, 2025), scheduled for launch in 2026, is expected to significantly increase the number of detected exoplanets. In addition, the Nancy Roman Space Telescope will be the first space mission with designated capabilities for direct imaging of exoplanets (Spergel et al. 2015; Akeson et al. 2019; Carrión-González et al. 2021). Kepler, TESS and PLATO rely on the transit method for planet detection, which is inherently biased towards small stars, large planets, and planets in close orbits. The large majority of small planets ($<1.5\ R_\oplus$) have periods below 100 days (e.g. Fulton and Petigura 2018). Detecting rocky worlds, especially around Sun-like stars, remains particularly challenging. The number of detected potentially-rocky planets with measured mass and radius — on which this article focuses — is currently limited to around $\sim$100.

1.1 Observed Parameters and Uncertainties

The key characteristics of exoplanets used to infer their interior structure and composition are their mass, measured with RV or transit timing variations (TTV), and radius, measured with transit photometry. However, the uncertainties in these measurements are strongly dependent on the precision of stellar properties. Stellar parameters impose strict limits on the achievable precision, with the best uncertainties being approximately 2% for stellar radius and 5–10% for stellar mass (e.g., Tayar et al. 2022). These values depend on the stellar type, age, and the detection method used. For young stars, typical uncertainties are larger, in the range of 10–20%. PLATO will use asteroseismic data and can provide stellar mass uncertainties as low as 1–3% (Rauer et al. 2014). In consequence, with PLATO, the best uncertainties on planet radii are 2–5% and 5–10% on planet mass using follow-up RV measurement campaigns, which implies uncertainty in mean density between 8–18%. Currently, typical well-characterised planets have uncertainties of 5–10% in radius and 10–30% in mass. Note, that only a small fraction of planets have both characterised radii and masses, about 3% (Jontof-Hutter 2019), which is due to the fact that transit measurements are generally independent from RV and TTV follow-up measurements. The planets with the best constrained parameters (including the rocky planet population) can be found in the PlanetS[2] catalog, recently updated by Parc et al. (2024).

Along with mass and radius also temperature can be estimated by using the orbital period and stellar luminosity. Due to observational biases in the transit and RV measurements, which favor the detection of planets on close-in orbits, most of the small planets detected so far are warm or hot worlds, with typical blackbody temperatures ranging between 500 and 2000 K (Fig. 1). By comparison, the melting temperatures of rocks lie between 1400 and 1900 K at 1 bar (see e.g., Takahashi 1986; Katz et al. 2003). It is important to note that any atmosphere surrounding a planet acts as a thermal blanket, potentially elevating surface temperatures above 2000 K. As a result, many small exoplanets may be lava worlds, with the surface dominated by a magma ocean rather than a solid mantle.

[1] https://exoplanetarchive.ipac.caltech.edu/

[2] https://dace.unige.ch/exoplanets/

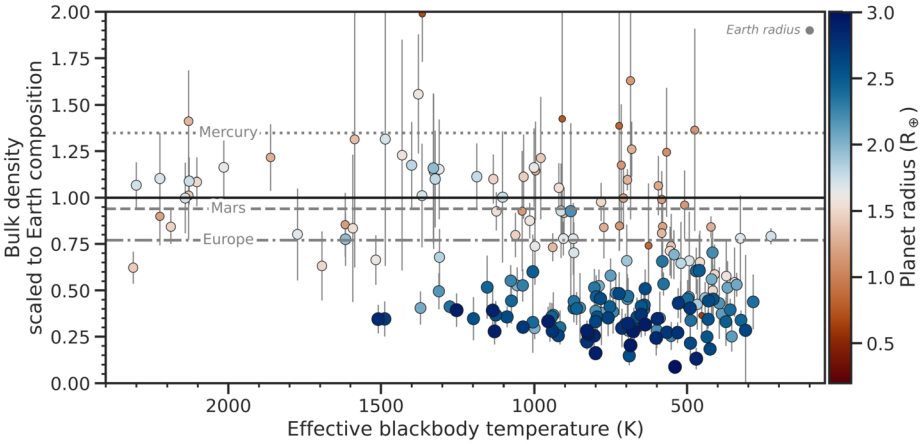

Fig. 1 Confirmed exoplanets with measured radius <3 $R_\oplus$ and measured mass <19 $M_\oplus$, excluding planets with mass uncertainty $>50\%$. Data are from the NASA Exoplanet Archive, accessed 05/12/2024, using the most recent entries for each planet. Effective blackbody temperature is calculated assuming 30% albedo. The y axis shows bulk density normalised to the bulk density of an Earth-like composition at that planet mass, which is calculated using the scaling $R_p/R_\oplus = \left(M_p/M_\oplus\right)^{0.282}$ (Zeng et al. 2019; Noack and Lasbleis 2020). Marker size is proportional to planet radius. Bluer (redder) colours indicate radii further above (below) 1.6 $R_\oplus$, which is an illustrative radius often taken to separate rocky planets from volatile-rich ones (Rogers 2015). Nonetheless, the scatter of blue markers denser than the Earth composition line and red markers less dense than this line shows that this 1.6 $R_\oplus$ 'boundary' is not hard

A few famous examples of temperate Earth-sized planets exist. The TRAPPIST-1 system, for example, harbours seven worlds around an ultracool red dwarf with equilibrium temperatures ranging from 400 K down to 170 K (Gillon et al. 2016, 2017). Thanks to intensive campaigns of transit observations and the resonant nature of the system (constraining transit timing variations), both the radii and the masses of the planets are known to a very good precision (Agol et al. 2021).

With the James Webb Space Telescope (JWST, Gardner et al. 2006), we are probing the upper atmospheres of exoplanets to higher precision. However, these atmospheric observations remain very challenging for rocky exoplanets, mainly because the signals from small planets are weak, while both stellar and instrumental noise are comparable in magnitudes. The activity of the stars complicates obtaining good spectroscopic data (Lim et al. 2023) but solutions might exist (Rathcke et al. 2025). As JWST works in the infrared, hot worlds (e.g., 55 Cnc e; Demory et al. 2011) and temperate worlds around small stars (e.g., TRAPPIST-1 b, c, and d, Greene et al. 2023; Lim et al. 2023; Zieba et al. 2023; Ducrot et al. 2025) are accessible for characterization. Note that in Greene et al. (2023), Zieba et al. (2023) and Ducrot et al. (2025), the technique used to assess the presence of an atmosphere was not relying on spectroscopy, but measuring the thermal emission during a secondary eclipse (when the planet passes behind the star). In principle, with JWST it is feasible, but challenging for rocky planets, to identify an existence of an atmosphere, and detect volatile species like CO_2, H_2O, CH_4, CO. The upcoming ARIEL (Atmospheric Remote-sensing Infrared Exoplanet Large-survey) mission (Tinetti et al. 2016; Beaulieu et al. 2018), scheduled to launch in 2029, will be limited to larger planets as its mirror is 3 times smaller than for JWST. Accordingly, for any in-depth characterisation of temperate Earth-sized planets, only future mission concepts like the Habitable Worlds Observatory (HWO, National Academies

of Sciences, Engineering, and Medicine 2023) and the Large Interferometer For Exoplanets (LIFE, Quanz et al. 2022) bring the necessary abilities to characterise temperate worlds.

2 The Diversity of Observed Exoplanets

Within the population of small exoplanets, observed bulk densities are diverse, though largely varying around Earth-like values (Fig. 1 and 3). These planets are categorised based on their bulk density as super-Earths or super-Mercuries, although the majority are likely more analogous to Venus because of their high stellar irradiation, making super-Venuses a more appropriate addition to the naming convention. There are several ways to explain density variations compared to Earth; i.e., higher amounts of volatiles (water), or higher/lower core mass fractions (see also the review by Jontof-Hutter 2019). In radius, the population is limited in practice by the so-called radius gap at 1.5–2.0 $R_\oplus$ (Sect. 2.1).

2.1 Radius Gap

The analysis of close-in planet radii with orbital periods within 100 days reveals a bimodal distribution, with two peaks at approximately 1.3 and 2.4 $R_\oplus$ (Owen and Wu 2013; Fulton et al. 2017; Owen and Wu 2017), which has been termed the "radius gap" or "radius valley" (Fig. 2). The radius gap is among the most important constraints on the interior compositions of super-Earths and the more low-density sub-Neptunes. The gap suggests that the population of super-Earths and sub-Neptunes is shaped by atmospheric loss to space of primordial gas envelopes (Owen and Schlichting 2024). This idea implies that a significant fraction of observed super-Earths started their evolution with a hydrogen-dominated envelope, contemporaneous with the protoplanetary disk (Owen 2019; Burn et al. 2024). Although these envelopes are quickly lost to space after the disk lifetime of few Myrs, we expect there to

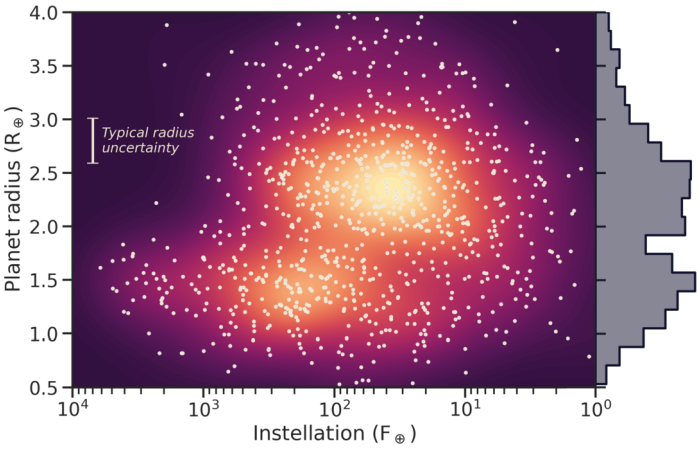

Fig. 2 Distribution of observed planets with orbital periods below 100 days as a function of received stellar flux (relative to Earth) and planet radius, showing two distinct populations of planets with a scarcity of planets between 1.5 and 2 $R_\oplus$. The background shows the corresponding density distribution (arbitrary units) using a kernel density estimation algorithm. The histogram on the right side shows the marginal density distribution of planet radii. Data are from the NASA Exoplanet Archive, accessed Oct 29, 2025, using the most recent entries for each planet. Only planets with a relative radius error below 10% are shown here

be lasting chemical imprints of any hydrogen-dominated envelope in contact with an early magma ocean. Endogenic production of water, up to ∼1 wt.%, is among the main consequences (Rogers et al. 2024). An early hydrogen envelope has been proposed even for Earth (Young et al. 2023), as it can fit fundamental features of the Earth (e.g., 'bulk redox state', core density) using a model of redox reactions between this hydrogen and a magma ocean.

2.2 Super-Mercuries

Most low-mass planets cluster around the bulk density of an Earth-like composition (Figs. 1 and 3). However, Fig. 1 also shows a number of planets with bulk densities similar to that of Mercury. Given that the radii of these planets are generally larger than the radius of Mercury, this population of planets is referred to as super-Mercuries (Marcus et al. 2010). Examples of such planets are GJ 367b and K2-229b, which both have a bulk density of ∼8000 kg m^{-3} (Santerne et al. 2018; Lam et al. 2021). Interior models suggest that these planets must host a substantial iron core in order to explain the high density (e.g., Wagner et al. 2012; Murgas et al. 2024). By comparing the bulk elemental abundance ratios of rocky planets to those of their host stars, it was shown that super-Mercuries orbit high metallicity stars (Liu and Ni 2023). It should be noted that the measurement errors can be large for both masses and radii, and the first planets assumed to be super-Mercuries have been revised to have lower bulk densities, owing to the ever growing observational baseline, general improvements in instrumentation, and improved determination of stellar parameters (e.g., due to the GAIA catalogue, Gaia Collaboration 2021). Figure 4 shows seven example planets with their observed density over time scaled to an Earth-like density, as well as a Mercury-like density for comparison (using scaling relationships from Noack et al. 2016). The first four planets (CoRoT-7b, Kepler-10b, K2-38b and K2-106b) are no longer believed to be super-Mercuries based on their revised planetary parameters. K2-229b and Kepler-406b, on the other hand, have both been first revised from Mercury-like to Earth-like in composition,

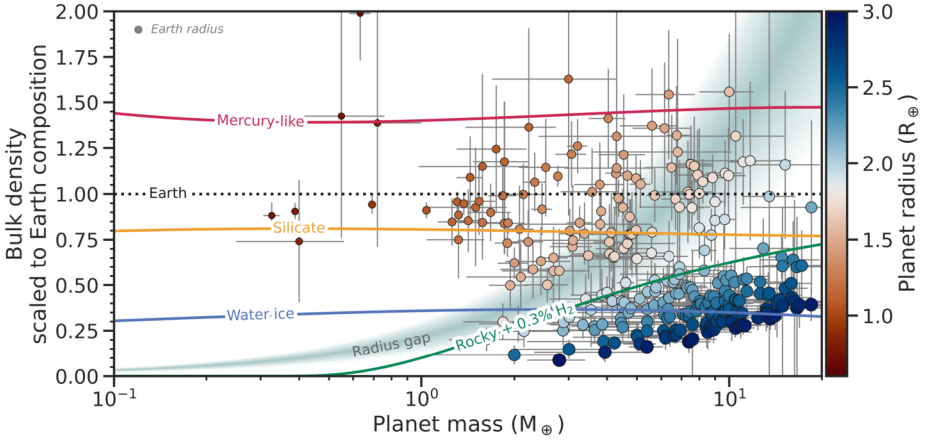

Fig. 3 The same as Fig. 1, but plotted in terms of planet mass. The coloured lines represent the density of a planet with constant composition: Mercury-like with a 70% iron core by mass (red, Baumeister and Tosi 2023); a theoretical pure-silicate body (yellow, Baumeister and Tosi 2023); a theoretical pure-water ice body (blue, Zeng et al. 2019); and a theoretical Earth-like composition with 0.3% H_2 by mass at 500 K (green, Zeng et al. 2019). The shaded area marks the location of the radius gap, assuming a nominal range between 1.5 and 2 $R_\oplus$ (Fulton et al. 2017)

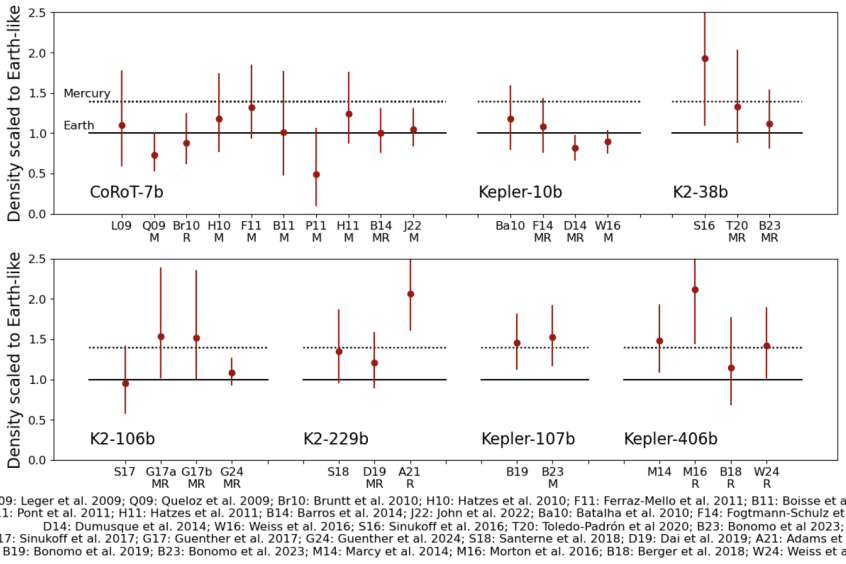

Fig. 4 Measured densities of seven different planets classified at least at some point in time as super-Mercuries in the literature, scaled to an Earth-like density and compared to a Mercury-like density (dotted lines). Labels on the x-axis refer to the respective publications; "M" refers to an update in the mass measurement and "R" for an update in the radius measurement

but newer measurements of their radii now suggest much denser compositions. Note that this can change again in the future as their masses have not been revised for several years. Similarly Kepler-107b only has two measurements of the mass and one measurement of the radius, so the planetary parameters may still be revised in the near future. The current sample of rocky exoplanets still includes several super-Mercuries with reproducible, accurate density measurements. However, Brinkman et al. (2024) highlight that uncertainty on the radius of the host star significantly influences the measured bulk density of small planets. As a matter of fact, using updated stellar properties, they find lower bulk densities for known super-Mercury candidates. In a similar vein, Rodríguez Martínez et al. (2023) reanalysed the observational data for K2-106 b to find a core mass fraction of $\sim 44^{+12}_{-15}\%$ (assuming an iron-free mantle), consistent with the core mass of Earth. Accordingly, Super-Mercuries might be less frequent than previously thought.

Multiple formation pathways can lead to the existence of super-Mercuries in theory. In one scenario, the planets form already iron-rich in a metal-enriched inner protoplanetary disk (Wurm et al. 2013; Johansen and Dorn 2022; Mah and Bitsch 2023). Alternatively, the planets may have initially formed with a core mass fraction similar to Earth, but lost parts of their mantle through processes such as mantle photoevaporation (Cameron 1985) or giant impacts (Benz et al. 1988; Reinhardt et al. 2022; Dou et al. 2024). Both the iron-rich formation theory and the photoevaporation theory predict that super-Mercuries should be the innermost planet in the system. Consequently, systems such as Kepler-107, where the iron-rich planet is not the innermost planet, are consistent with formation by giant impacts (Bonomo et al. 2019; Cambioni et al. 2025). However, Cambioni et al. (2025) also find that the rates of mantle-stripping giant impacts is likely not sufficient to explain the sizes and abundance of observed super-Mercuries.

3 Interior Modelling of Rocky Planets

Interior models are an integral part in the characterization of exoplanets, providing the connecting link between observations and geophysical interpretations. To provide insights into planets' interior compositions and structures, properties of observed exoplanets (e.g., mass and radius) are compared to the same properties calculated for synthetic exoplanets. Such models consider the planets as spherical symmetric and in hydrostatic equilibrium. Differential equations to represent the profiles of mass, radius, density and temperature are solved using the physiochemical properties of chosen mineralogical phases (Duffy et al. 2015). The latter may be a product of thermodynamic modelling starting from a bulk elemental composition, or instead chosen *a priori*. Models often consist of planets with an arbitrarily layered structure and interior mineralogy which mimic solar system planets. A considerable number of interior codes have been developed over the years (e.g., Sotin et al. 2007; Seager et al. 2007; Valencia et al. 2007; Rogers and Seager 2010; Wagner et al. 2011; Dorn et al. 2015, 2017b; Hinkel and Unterborn 2018; Unterborn and Panero 2019; Baumeister et al. 2020; Huang et al. 2022, see also Sect. 3.3).

Challenges in modelling exoplanets' interiors remain due to an inherent degeneracy between composition and bulk density. Planets with very different internal structures and mineralogies can be represented by the same calculated mass and radius, hampering a unique interpretation of the observations (Valencia et al. 2007; Zeng and Seager 2008; Rogers and Seager 2010, see Sect. 4.1). Using other constraints — for example, stellar composition (Sect. 5.1) — can help to reduce the degeneracies (Dorn et al. 2015, 2017b,a), but a unique solution will likely never be attainable (Sect. 4.1). Understanding planetary interior structure and composition is even difficult for the Earth, where we have indirect evidence from seismology, and for solar system planets, where space missions can provide additional data such as Love numbers (e.g., Park et al. 2025, and Sect. 4.1).

In any case, to take strides towards a more accurate interpretation of planetary and exoplanetary interiors we should not forget the role of experimental studies. A wide array of high pressure and temperature experiments as well as analytical techniques have been developed to investigate and constrain the properties of geomaterials, the building blocks of any planet. Their characteristics control all the aspects of a planet, from how it is structured, to its possible large scale properties (e.g., the presence of an atmosphere or a magnetic field) and are a vital component of all the models used in the field, from mass-radius models to dynamic and thermal evolution models. In the next section we will review how equations of state are used with mass-radius models as an example for the role of material properties in the interpretation of observations. In Sect. 4.2, we discuss the uncertainties on experimental equation of state measurements and how they affect models.

3.1 Equations of State and High-Pressure Physics

Rocky planets are made of condensed matter (minerals and/or Fe-rich metals). As such, it is necessary to consider the bonding environment of atoms and the internal energy associated with atom-atom interaction. Accordingly, at the heart of every planet model sit equations of state (EoS) and thermal models, which encapsulate the physics of mineralogical phases under planetary interior conditions. They describe how the volume V (or equivalently the density) of a material varies with pressure and temperature. In a solid, the amount of compression with pressure P and temperature T is characterised by the (isothermal) bulk modulus $K_T = -V\partial P/\partial V$ and its first and second derivatives $K_T' = -\partial K_T/\partial P$ and $K_T'' = -\partial^2 K_T/\partial P^2$.

EoS describe the change in volume with pressure; they are polynomials, and in certain cases their complexity can increase depending on where the polynomial is truncated. The main terms are the zero-pressure volume (V_0) and the bulk modulus (K_0) in the simplest polynomial. The first and second derivatives of the bulk modulus with pressure (i.e., K_0' and K_0'') can be added if the simple formulation does not accurately represent the dataset. The simplest way to account for temperature-induced changes in the volume is to apply a thermal expansion term to a previously determined ambient-temperature EoS. In reality, as pressure and temperature have a simultaneous effect of shrinking and inflating the unit cell volume, it is more accurate to account for both the effects in the parameterization of volume variations, and hence use a P-V-T EoS that includes also a thermal model (e.g., Mie-Grüneisen-Debye, or the thermal pressure). Over the years, many formalisms have been defined to parameterize equations of state, thermal expansion, and P-V-T EoS. While a precise description of all of the models is beyond the scope of this paper, additional details can be found in Angel (2000), Kroll et al. (2012), Poirier (2003), and Angel et al. (2018).

Rocky planets are made up of a wide range of mineral phases, each with their own specific EoS parameters. In such cases, the equations of state of the different mineralogical phases need to be combined, which can be done in different ways. For example, with the additive-volume rule, the density ρ_m of a mineral assemblage can be expressed in terms of the individual densities ρ_i of every species i,

$$\rho_m = \left(\sum_i \frac{w_i}{\rho_i} \right)^{-1}, \tag{1}$$

where w_i is the respective weight fraction. The validity of this mixing rule has been experimentally validated at high pressures and temperatures (Bradley et al. 2018).

All EoS are based on specific thermodynamic assumptions. There is no absolute basis for defining the correct form of EoS for solids. In that regard, all EoS we use in planetary interior modelling are approximations, and depend on the data used for the parametrization. This means that, in general, there is no "correct" choice of EoS. The validity of EoS depends on how well they fit the data; each formulation is individual because that specific set of parameters represent the best fit for the data at hand. Accordingly, the parameters from one EoS should generally not be used in another EoS formulation and it should be noted that EoS for the same materials can change and improve in time; for example, if another dataset with a higher pressure and temperature extension gets collected. In a similar manner, EoS defined for solids are generally not applicable to materials at temperatures above their melting temperature. Many of the EoS and thermal models available in literature for planetary materials are based on experiments where volume data are collected at either high pressure, high temperature, or simultaneous at both high pressure and temperature. As a consequence, the extension of the pressure and temperature range in which the materials' properties are explored strongly depends upon technological developments.

Experimental techniques to study EoS (i.e., density changes with pressure and temperature) have made major advances due to the improved techniques of high-pressure generation and of the measurements of density change under pressure using synchrotron X-ray (Fig. 5). EoS of materials have been routinely determined experimentally down to the conditions equivalent to Earth's deep lower mantle and core by static compression — e.g., to ~120 GPa and ~2500 K for mantle minerals (Tange et al. 2012) and ~330 GPa and ~3000 K for core materials (Tateno et al. 2010). It is now possible to reach higher pressures and temperatures (~600 GPa, ~14,000 K) with shock compression experiments (e.g., Wicks et al. 2024; Duffy and Smith 2019). However, the complexity of such experiments, and the existence

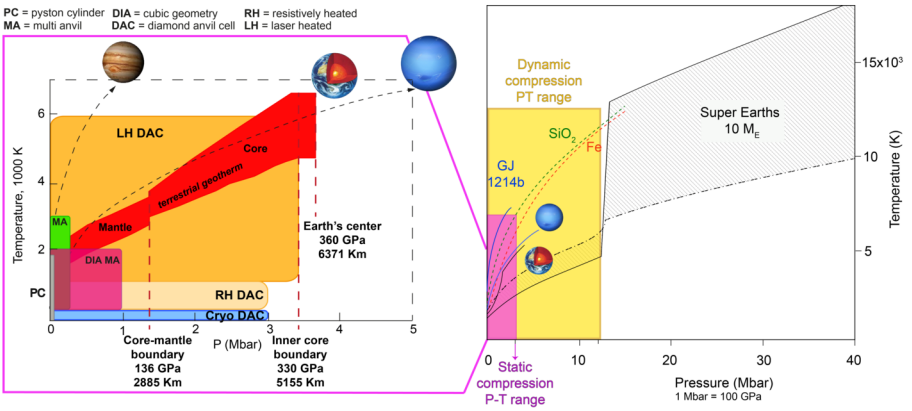

Fig. 5 Pressure-temperature diagrams illustrating the ranges covered by the available experimental techniques along with some references for solar system planets and exoplanets. The figure on the right is modified from Duffy and Smith (2019)

of few facilites where they can be performed, makes it harder to produce results for a wide set of materials. For a detailed review of high pressure techniques, see e.g., Fei and Tracy (2025).

In principle, experimental data collected by different authors on the same material can be combined to obtain a single equation of state, as long as the datasets are consistent. This practice is commonly used by experimentalists to see how well their collected datasets compare to other. However, attention should be given to all the experimental details, especially for diamond anvil cell studies, as the experimental setup might have an effect on the measured data. More importantly, if multiple datasets are combined, the equations of state cannot be stitched together using values for the parameters from different works. It is more appropriate to combine all the data (e.g., P-V-T data) and fit the desired equation of state.

In recent years, substantial progress in computational mineral physics has also made it possible to determine EoS with numerical calculations. This technique allows reaching large compression states, including conditions that have never been achieved in the laboratory (e.g., Tsuchiya and Kawai 2013). Ab initio methods provide a technique to numerically calculate high-pressure and -temperature properties of materials on a first-principles basis, starting from the fundamental quantum mechanical laws without introducing empirical parameters. Density Functional Theory (DFT) calculations are a widely used ab initio method to calculate the EoS of materials under extreme conditions. DFT allows the description of the structure and thermodynamic properties of materials at the atomic level, including phase diagrams, thermoelastic properties, and melting curves. DFT-derived EoS can typically not be represented by an analytical closed-form equation but are instead tabulated and interpolated between discrete data points.

Finally, upon larger compression in the TPa regime, atom to atom interaction is no longer driven by the interaction between outer electrons. There is no distinction between outer and inner electrons; atoms lose their identity (Al'tshuler and Bakanova 1969). In this regime, most of the free energy of given materials is in electrons that would occupy the same energy level (the Fermi level), and these materials follow a different EoS called the Thomas-Fermi EoS (e.g., Poirier 2003). Since the basic physics controlling the density in this regime differ from the physics operating at lower pressures, the mass-radius relation in this regime

differs substantially from the mass-radius relation at lower pressures: close to $R \propto M^{\frac{1}{3}}$ at low pressures, while $R \propto M^{-\frac{1}{3}}$ at high pressures (Thomas-Fermi EoS). Most rocky planets belong to the low-pressure regime, whereas the largest giant planets would belong to the Thomas-Fermi regime.

On a side note, models of giant planets typically do not distinguish between separate silicate and iron layers, and model the "rocky" cores as a homogeneous mixture of both (e.g., Hubbard and Marley 1989; Nettelmann et al. 2008). In fact, there may not even be a clear transition between rocky core and the surrounding volatile-rich envelope, as the respective materials may become miscible at the pressure and temperature conditions inside giant planets (see e.g., Vazan et al. 2022; Young et al. 2024; Benneke et al. 2024).

3.2 The Choice of Temperature Profile

When modelling the interior of a planet, a choice has to be made on how to define the temperature profile. Temperature profiles are tightly linked to materials' thermal and transport properties (i.e., the way in which materials transfer heat). While the former (e.g., thermal expansivity) can be obtained fitting a P-V-T EoS to a set of P-V-T data, the latter represent one of the major sources of uncertainty because they are much harder to determine. Experiments are challenging, as they require being able to control and probe a field (i.e., electrical, magnetic, temperature) gradient. Only few groups have the capability of doing thermal conductivity experiments and to this date, not many mineralogical phases have been studied. Additionally, for some of the studied phases, there are discrepancies in the results obtained by different groups (e.g., for pure Fe; Konôpková et al. 2016; Ohta et al. 2016; Hasegawa et al. 2024).

The interiors of rocky planets are much hotter than their surfaces, due to the large amount of heat left over from their formation, and the continuous production of heat through the decay of long-lived radionuclides. In addition, planets are very efficient at retaining this heat, in particular for planets more massive than Earth (Stixrude 2014). Furthermore, iron cores are expected to be super-heated with respect to mantles because a large fraction of the gravitational energy during formation is transported to the core itself by sinking of iron-rich material. As convection in the core cannot penetrate the core-mantle boundary (CMB) layer, core cooling is further limited to conduction through the CMB (Stixrude 2014).

How can we estimate the mantle and core temperatures of a planet? Stixrude (2014) argues that the temperature state of rocky planets is governed by silicate melting. Cooling of a planet via melt extraction is efficient, so the top of the mantle should cool until the solidus curve is reached and cooling becomes inefficient. A similar argument can be made for the temperature at the core-mantle boundary: if the core temperature were above the solidus of the silicate mantle, a large-scale magma ocean would quickly form whose low viscosity would efficiently cool the core (Gaidos et al. 2010). Following Stixrude (2014), the temperature T_{CMB} at the core-mantle boundary (in K) can be estimated as

$$T_{\mathrm{CMB}} = 5400(1 - \ln x_0)^{-1} \left(\frac{P_{\mathrm{CMB}}}{140\ \mathrm{GPa}} \right)^{0.48}, \tag{2}$$

where P_{CMB} is the pressure at the CMB in GPa, and x_0 is the mole fraction of $MgSiO_3$ in the mantle. A value of $x_0 = 0.79$ produces the solidus of an Earth-like mantle composition.

Inside a planet, heat is transported through convection in the solid mantle and liquid core (for an in-depth look, see also Lourenço et al., this collection). Heat transfer in and out of a convecting parcel of material by diffusion is much slower than the typical convective time

scales, making temperature changes a nearly adiabatic process. Thus, an adiabatic temperature profile is a typical assumption in interior models, with the temperature gradient over radius r given as

$$\frac{\mathrm{d}T}{\mathrm{d}r} = -\frac{\alpha g T}{c_p}, \tag{3}$$

where α is the thermal expansion coefficient, c_p is the specific heat capacity, and g is the gravitational acceleration. Note here that α and c_p are material specific, and also vary with pressure and temperature. Likewise, g is not constant throughout the planet (although it is nearly constant in Earth's mantle, see e.g., Dziewonski and Anderson 1981).

Using and adiabatic temperature profile always comes with the implicit assumption that efficient convection is ongoing within the planet core and mantle. However, the rheologies, i.e., the flow behaviour of minerals, of exoplanets with different mineralogy to Earth and at the temperature and pressure conditions of super-Earths are not well understood. Several studies have shown that the interior dynamics may be significantly different to that of Earth, for example due to the formation of a thick non-convective layer at the core-mantle boundary for planets more massive than Earth (Stamenković et al. 2012), or by developing a stable mantle stratification with two convection layers (Spaargaren et al. 2020).

Mixing length theory (MLT) provides an alternative to needing to assume an adiabatic temperature profile (Wagner et al. 2011, 2012). MLT provides an estimate of the (local) convective heat flux by considering the distance a fluid parcel can move before it dissipates its thermal energy. It thus provides a way to self-consistently calculate the temperature at every point within the mantle.

Fortunately for interior modelers, the exact temperature profile plays only a minor role in controlling the bulk density of a rocky planet, and thus has only little effect on planet characterization (see, e.g., Seager et al. 2007; Dorn et al. 2015; Unterborn et al. 2016; Thomas and Madhusudhan 2016; Hakim et al. 2018). The underlying physical reason for this is that in rocky bodies, atom-atom interactions dominate the internal energy, and thus the density depends only weakly on temperature. Instead, density in rocky planets is largely determined by pressure. This stands in contrast to gas giants, where entropy is an important part of the internal energy, and hence density is particularly sensitive to temperature. As such, temperature can have a significant effect on the inferred mass and thickness of the volatile-rich layers of a planet; for example, water oceans (Thomas and Madhusudhan 2016) or extended atmospheres (e.g., Nixon and Madhusudhan 2021).

We can estimate the first-order effect of temperature on a rocky planet's radius by assessing how the bulk density changes as a function of temperature. The temperature effect on density can be well described using the thermal expansion coefficient α (Fei 1995; Angel 2000):

$$\rho(T) = \rho(T_0) \exp \int_T^{T_0} \alpha(T)\, dT, \tag{4}$$

where $\rho(T_0)$ is the density at the reference temperature T_0 (typically room temperature). Assuming a constant α, this reduces to

$$\rho(T) = \rho(T_0) \exp\left[-\alpha(T - T_0)\right]. \tag{5}$$

Taking a characteristic value of $\alpha = 2 \times 10^{-5}\ \mathrm{K}^{-1}$ for both mantle minerals and the iron core, an 1000 K increase in the average temperature of the planet decreases the planet bulk

density by about 2%, for an equivalent radius increase of only about 0.7% (see also Noack and Lasbleis 2020; Foley et al. 2020).

However, it is to note that the temperature structure of a planet has profound consequences for its thermal evolution, the emergence of a magnetic field, and its tectonic state (see also Lourenço et al., this collection, for an in-depth exploration of the thermal evolution of planets).

3.3 Tools for Interior Characterization

Mass-radius scaling laws have long formed a cornerstone of exoplanet interior modelling. Mass-radius composition curves can be well approximated by power laws in the form of

$$\mathrm{R} \propto \mathrm{M}^{\beta}, \tag{6}$$

with the exponent β typically derived by fitting the power law to interior models. For rocky planets, typical values for β are between $0.25 - 0.3$ (e.g., Valencia et al. 2006; Sotin et al. 2007; Wagner et al. 2011; Noack and Lasbleis 2020).

Over the years, these scaling laws have seen various extensions, with additional parameters such as planet bulk iron content (Noack and Lasbleis 2020), core mass fraction (Zeng et al. 2016), or water content and instellation (Turbet et al. 2020).

As the field matured, so did the software and models available to the community, in particular in open-source codes which aim to help in the characterization of planet interiors. We aim to provide here a comprehensive overview of the ones which are of the most interest for the characterization of rocky planets and for exploring the boundaries of the population of rocky planets. Codes can be broadly categorised into four areas of application: Interior structure modelling, interior retrievals, bulk parameter estimation, and visualization. A summary of these codes with their respective links is given in Table 1.

Interior structure codes simulate the radial structure of a planet, such as density and temperature profiles (see Sect. 3). *MAGRATHEA* (Huang et al. 2022) is a general interior structure code written in C++ and supports up to 4 planetary layers: core, mantle, hydrosphere, and atmosphere. *ExoPlex* (Unterborn et al. 2023) is a thermodynamically consistent interior structure model written specifically for predominantly rocky planets, taking into account mantle mineralogy and core chemistry, for example the fractionation of iron between mantle and core. *ExoPlex* utilizes the *BurnMan* toolkit (Myhill et al. 2023), a mineral physics framework for rocky planets. *BurnMan* itself allows modelling of interior structures as well. *ROWS* (Noack and Lasbleis 2020) is 1D model to calculate the internal structure and depth-dependent thermodynamic parameters for rocky planets and ocean worlds. *GASTLI* (Acuña et al. 2024) is an interior model which, while designed primarily for gas giants, can also model planets with extended gas and water envelopes.

Planet composition and interior retrieval tools aim to determine the interior composition of exoplanets based on observable bulk parameters, or try to estimate the compositional ranges, for example from the bulk stellar abundances. The interior structure codes *MAGRATHEA*, *ExoPlex*, and *GASTLI* already include inbuilt interior retrieval capabilities. A few codes exist to estimate the distribution of individual planet interior layers: *HARD-CORE* (Suissa et al. 2018) is a parametric model to estimate the minimum and maximum core size of planets, while *SMINT* (Piaulet et al. 2021) provides distributions for hydrogen and water envelope mass fractions. *SuperEarth.py* (Plotnykov and Valencia 2020) is an analytical model based on the *SuperEarth* code (Valencia et al. 2006, 2007) to estimate iron core mass and Fe/Si ratio of a given planet, or to estimate mass or radius given stellar Fe/Si constraints. *exopie* (Plotnykov and Valencia 2024) estimates core mass fraction of rocky planets,

Table 1 Open-source codes for modelling and characterising low-mass exoplanets

Code	Link	Reference
Interior structure models		
MAGRATHEA	github.com/Huang-CL/Magrathea	Huang et al. (2022)
General 1D structure model supporting planets with core, mantle, hydrosphere, and atmosphere.		
ExoPlex	github.com/CaymanUnterborn/ExoPlex	Unterborn et al. (2023)
Thermodynamically self-consistent interior model for rocky planets.		
BurnMan	github.com/geodynamics/burnman	Myhill et al. (2023)
Mineral physics framework for modelling planetary interiors.		
GASTLI	github.com/lorenaacuna/GASTLI	Acuña et al. (2024)
A coupled interior-atmosphere model for mini-Neptunes and gas giants.		
ROWS	github.com/FUB-Planetary-Geodynamics/ROWS_Interior-Structure-Model	Noack and Lasbleis (2020)
A Python tool for modelling the internal structure of rocky planets and ocean worlds.		
Planet composition and interior retrieval tools		
HARDCORE	github.com/gsuissa/hardCORE	Suissa et al. (2018)
Estimates minimum and maximum core sizes of planets.		
SMINT	github.com/cpiaulet/smint	Piaulet et al. (2021)
Posterior distributions for H/He and H_2O mass fractions.		
SuperEarth.py	github.com/mplotnyko/SuperEarth.py	Plotnykov and Valencia (2020)
An analytical model for calculating the interior parameters of exoplanets.		
exopie	github.com/mplotnyko/exopie	Plotnykov and Valencia (2024)
Find the interior structure error of core, water, or atmospheric mass fractions.		
ExoMDN	github.com/philippbaumeister/ExoMDN	Baumeister and Tosi (2023)
Fast interior retrievals with neural networks		
plaNETic	github.com/joannegger/plaNETic	Egger et al. (2024)
Neural network-based Bayesian interior retrieval framework.		
ExoInt	github.com/astro-seanwhy/ExoInt	Wang et al. (2019c)
Devolatilize stellar abundances to produce rocky bulk composition.		
ECCOplanets	github.com/AninaTimmermann/ECCOplanets	Timmermann et al. (2023)
Equilibrium condensation code to determine rocky composition from stellar abundances.		
Bulk parameter estimation and population fitting tools		
spright	github.com/hpparvi/spright	Parviainen et al. (2023)
Predicts planetary masses, densities, and RV semi-amplitudes from radii (or vice versa).		
Forecaster	github.com/chenjj2/forecaster	Chen and Kipping (2017)
Estimates mass from radius (or vice versa) using probabilistic mass-radius relations.		
BEM	github.com/soleneulmer/bem	Ulmer-Moll et al. (2019)
Predicts planetary radii based on bulk planetary and stellar parameters.		
MRExo	github.com/shbhuk/mrexo	Kanodia et al. (2019)
Nonparametric probabilistic framework to model planet populations using up to four observables.		
EvapMass	github.com/jo276/EvapMass	Owen and Campos Estrada (2020)
Predicts minimum masses of mini-Neptunes in multi-planet systems.		

Table 1 (*Continued*)

Code	Link	Reference
Visualization tools		
mr-plotter	github.com/castro-gzlz/mr-plotter	Castro-González et al. (2023)
Mass-radius diagram plotting tool.		
MARDIGRAS	github.com/an0wen/MARDIGRAS	Aguichine (2024)
Interactive mass-radius relationship visualization tool.		
exoplanet	github.com/astrozeng/exoplanet	Zeng et al. (2021)
Mathematica tool to plot exoplanet data and histograms in the mass-radius diagram.		
pyExoRaMa	github.com/francescoa97outlook/pyExoRaMa	Francesco and Mario (2022)
Interactive tool to investigate the radius-mass diagram, based on the tool by Zeng et al. (2021).		

and water mass fraction of water worlds, along with their respective uncertainties. For full Bayesian interior retrievals, *ExoMDN* (Baumeister and Tosi 2023) and *plaNETic* (Egger et al. 2024) are publicly available fast machine-learning based models. Going beyond mass and radius of an exoplanet, *ExoInt* (Wang et al. 2019c) and *ECCOplanets* (Timmermann et al. 2023) are two codes to estimate the bulk planet composition from stellar abundances.

Bulk parameter estimation tools aim to predict unobserved bulk planet parameters, typically relying on the observed population of planets. This includes for example estimating the mass of a planet based on its radius, or vice versa. Most of these work in a probabilistic way to estimate the posterior distributions of unseen parameters, using the observed population of exoplanets as a basis, for example *Forecaster* (Chen and Kipping 2017), *BEM* (Ulmer-Moll et al. 2019), *MRExo* (Kanodia et al. 2019), and *spright* (Parviainen et al. 2023). In a way, these tools represent more sophisticated, multi-dimensional, non-parametric versions of the mass-radius relations and scaling laws. In addition, for multi-planet systems with planets both above and below the radius gap, *EvapMass* (Owen and Campos Estrada 2020) allows estimations of the minimum masses of planets above the radius gap.

Lastly, a few open-source tools exist which aid not directly in modelling of planets, but instead in the *visualization* of exoplanet data. *mr-plotter* (Castro-González et al. 2023) and *MARDIGRAS* (Aguichine 2024) are Python-based tools to generate mass-radius plots. A similar tool, named *exoplanet*, exists for Mathematica (Zeng et al. 2021), and has also been translated to Python (*pyExoRaMa*, Francesco and Mario 2022).

4 The Perils of Planet Categorisation

As the articles of this collection deal primarily with the geophysics of rocky exoplanets, it is reasonable to ask how we can actually determine if an observed planet is rocky in nature or not. A first remark to make is that bulk density alone is not a good indicator of planet composition due to the compression of planetary materials at high pressures. Earth has a bulk density of 5515 $\mathrm{kg\,m^{-3}}$. A 10 Earth mass planet with the same relative core size and composition as Earth would have a bulk density of about 8500 $\mathrm{kg\,m^{-3}}$ (here calculated with the parametrizations from Noack and Lasbleis 2020), which is more than that of pure iron at room temperature and pressure. Some degree of interior modelling incorporating high-pressure physics is therefore necessary to reliably determine the make-up of a planet.

The term "rocky planet" is not well defined. Should we still call a planet with a 100 km deep water ocean rocky? Similarly, how big can a planet's atmosphere be before the planet no longer classifies as rocky? For the purposes of this review, we adopt a practical definition: a rocky planet is one consisting primarily of silicate minerals and metals, with an amount of surface water not sufficient to affect the observed mass, and a relatively thin atmosphere with respect to planet radius. Based on this definition, we exclude sub-Neptunes with rocky cores but thick H_2 atmospheres. A super-Mercury (see Sect. 2.2) on the other hand with a predominantly metallic composition would be considered rocky.

Computed mass-radius relations (or mass-density relations, see Fig. 3) can give us a first estimate of the nature of the planet. Planets above the line for (i.e., less dense than) a pure silicate composition must contain some amount of volatiles, be it in the form of a water/ice layer or an extended atmosphere, or incorporated into the mantle (although this has only a secondary effect on mass and radius, Shah et al. 2021) and core. Here lies one of the limitations of this method: since we do not know the exact composition and mineralogy of the planet, there is no single composition line which can divide between the volatile-rich and rocky planets. Furthermore, a planet sitting below the line of (i.e., denser than) pure silicate composition may yet have significant amounts of volatiles. A thick atmosphere or water layer may be masked by an iron core, which compensates for the low density of the volatiles. In terms of bulk density, which is what the mass-radius curves in effect depict, this scenario can masquerade as a pure silicate planet.

As we have seen in Sect. 3.2, temperature has only little effect on the bulk density of a rocky planet. However, surface temperature can affect the observed bulk density, even for a rocky planet, if this temperature is high enough for most of the mantle to be sustained in a molten state. This particular scenario could be relevant for very young planets of Earth-size or larger. In this scenario, sufficient water may dissolve into the magma to cause a radius inflation. Studies have predicted such a density variation up to several percent for a given bulk composition (Dorn and Lichtenberg 2021). However, details about the solubility of water and hydrogen in magma oceans are missing, hampering a realistic assessment of the radius inflation induced by volatile intake.

In that regard, mass-radius curves are most valuable for population-wide studies, such as trying to find compositional trends in observed planets, and less so in characterising the composition of individual planets. When applied to individual planets, we quickly run into the problem that the number of unknown parameters is larger than the constraining observables. This leads to the non-uniqueness problem (interior structure degeneracy), where many possible interior structures fit a given planet (Sect. 4.1).

In spite of this long-known mass-radius-composition degeneracy (e.g., Seager et al. 2007; Valencia et al. 2007; Elkins-Tanton and Seager 2008), exoplanet researchers have sought to map out the boundaries in mass-radius space (or, sometimes, only one of the two) that might be used to delineate "rocky" planets. To this end, the curve of pure $MgSiO_3$ has been more-or-less accepted as a hypothetical end-member composition for the least-dense rocky planet (e.g., Rogers 2015). Even then, however, planets overabundant in CaO and Al_2O_3 due to extreme high-temperature condensation could in principle be less dense than $MgSiO_3$ (Dorn et al. 2019). Otherwise, for the majority of exoplanets, it is difficult to conceive of formation scenarios that would create a world virtually free of iron (as metal or oxide). Considering the observed distribution of stellar Fe abundances, among other compositional variables, Unterborn et al. (2023) suggest a slightly denser mass-radius curve as a limit to "nominally rocky" planets, with the scaling relationship $M/M_\oplus = 0.19 + 0.64\,(R/R_\oplus)^{4.1}$. They note nevertheless that anomalously Fe-poor bulk compositions could place a rocky planet out of this bound. In summary, it remains likely that a planet less dense than $MgSiO_3$

is *not* rocky. As bulk density increases towards pure Fe, a planet's rocky nature might be said to become qualitatively likelier, yet for intermediate bulk densities, attempting such a categorisation benefits from other information (e.g., very high equilibrium temperatures prohibiting volatile retention).

In reality, many known exoplanets are not detected in both transit and radial velocity, and only one of mass or radius is measured. Considering this population, it would be convenient to have a "rocky planet cutoff" in terms of mass or radius alone. The radius gap (Sect. 2.1) temptingly points to such a cutoff in radius: somewhere between 1.5 and 2.0 $R_\oplus$, but most widely interpreted to be at 1.6 $R_\oplus$. Indeed, several years before this radius gap was pointed out (Fulton et al. 2017), a statistical study by Rogers (2015) independently identified $\sim$1.6 $R_\oplus$ as the point where 50% of planets in the *Kepler* sample of the time are less dense than pure $MgSiO_3$. However, if needing to apply this rule-of-thumb, it is important to recognise the intention of Rogers (2015) that this cutoff is not a *hard* one. Figure 1 provides a simple illustration of the density scatter around 1.6 $R_\oplus$: there are planets $<$1.6 $R_\oplus$ with uncompressed density closer to Europa ($>$7% ice by mass; Gomez Casajus et al. 2021); there are planets $>$1.6 $R_\oplus$ relatively denser than Earth. A corollary is that predicting an unknown mass from a known radius — using a scaling relationship or other statistical method — may bring misleading results. Overall, although the radius gap may *broadly* separate rocky exoplanets from volatile-rich ones at a population level, classifying an individual planet is best treated with caution.

Given the inconclusiveness of a radius-only cutoff towards placing an individual planet in a categorical box, applying a mass-only cutoff is even more challenging, if only because mass increases much faster than radius for a line of constant bulk composition. A small discrepancy in mass is associated with a very large change in radius, so even more mass-radius-curve intersections become possible. Labelling a planet as rocky based on mass alone is unlikely to be informative.

4.1 The Non-uniqueness Problem and Ways to Ameliorate It

As seen in Sect. 3, interior models allow us to build accurate descriptions of the interior of planets, given that we know of the basic setup of the planet: its mineralogy and bulk composition. This is a *forward* problem that is straightforward to handle. However, when observing a planet, we are facing an *inverse* problem: we do not have observational access to the parameters which need to be prescribed in the interior models, and the goal is to recover, from a given set of observational data, the corresponding interior/model parameters which reproduce the observations. Inverse problems are notoriously difficult to solve.

In the Solar System, a wealth of data is available to help constrain the interior of the planets. Measurements of the gravitational moments constrain the mass distribution inside the planets. Seismic measurements on Earth, the Moon, and Mars allow a determination of the size of the iron core. Chemical analysis of surface material and measurements of the surface heat flow, for example from the InSight lander on Mars or the Apollo missions, allow further inferences on the material properties and interior conditions of the terrestrial planets. Even despite all this, we still do not have a clear view of the interior structure and chemistry of many Solar System bodies. For example, while we can make some inferences on the core size of Venus based on its similarities to Earth, there is still no definitive answer for the size of Venus' core.

It is an even more difficult situation with exoplanets. The measurements we are able to make of Solar System bodies are largely unavailable. As discussed throughout, exoplanet measurements are mostly limited to the basic bulk planetary parameters such as mass, radius,

and, consequently, bulk density, in addition all carrying potentially substantial measurement uncertainty. As a result, exoplanet interior models are inherently non-unique, because the large number of unknown parameters outweigh the limited amount of observables. One set of observable parameters can correspond to a multitude of possible planet interior scenarios (e.g., Valencia et al. 2007; Zeng and Seager 2008; Rogers and Seager 2010; Dorn et al. 2015, 2017b; Baumeister et al. 2020; Zhao and Ni 2021; Baumeister and Tosi 2023; Haldemann et al. 2024). The amount of inherent unknowns about an exoplanet interior is enormous: We do not know *a priori* the bulk composition of the planet, if it has water on the surface, if it has an atmosphere, what the composition of the atmosphere is, what the mantle mineralogy is, how much light elements there are in the iron core, and so on. Further constraints are needed to properly reduce this non-uniqueness, and precise measurements of the mass and radius are necessary to have a chance at constraining the interior (e.g., Baumeister and Tosi 2023; Plotnykov and Valencia 2024).

In a more mathematical sense, the goal of an inverse problem is to find the conditional probability distribution $p(\mathbf{m} \mid \mathbf{o})$ (i.e., the uncertainty) of the unknown model parameters $\mathbf{m}$ (e.g., the mass of the iron core, thickness of an atmosphere) given observed parameters $\mathbf{o}$ (e.g., planet mass and radius). Bayesian inference models, using sampling algorithms such as Markov-chain Monte-Carlo (e.g., Rogers and Seager 2010; Dorn et al. 2015, 2017b; Acuña et al. 2021), provide a way to sample $p(\mathbf{m} \mid \mathbf{o})$ and thus help to quantify the range of interior structures that fit an observed planet, while also directly including model and observational uncertainties. However, these models are typically slow and computationally expensive, as typically several hundred thousand interior structures need to be calculated to explore the parameter space of a single planet. In recent years, machine learning methods have been employed to speed up interior retrievals (e.g., Baumeister et al. 2020; Baumeister and Tosi 2023; Haldemann et al. 2023; Egger et al. 2024).

There is some additional information beyond mass and radius that, if invoked, can help constrain the "rocky mass fraction" of an exoplanet. The most commonly-used extra piece of evidence follows a working assumption that planets and their host stars have similar refractory and moderately volatile element abundances (e.g., Santos et al. 2015; Dorn et al. 2017a,b; Plotnykov and Valencia 2024). If we presume such a correlation, if we have a measurement of Mg/Fe or Si/Fe in the stellar photosphere, then this measurement can be used as prior information on the bulk planet iron-to-silicate ratio (Sect. 5.1).

In this way, varying stellar elemental abundances is one axis of potential exoplanet compositional diversity. Having some idea of what bulk compositions to expect is informative in a Bayesian sense; it can serve as a reality check on choosing what materials to include in an interior structure model or parameter sweep. Whilst the details of an exoplanet's interior chemistry will always elude us to a (likely large) degree, Sect. 5 will review current expectations of rocky planet compositional diversity and how it could be used to constrain planetary interior structure.

Lastly, a tangential but very strong indicator of the rocky nature of a hot, tidally-locked planet is the non-detection of an atmosphere from photometric phase curve observations. Phase curves reveal the hemispheric temperature contrast between the permanent dayside and nightside of the planet. A sufficiently-large temperature contrast indicates no heat redistribution, hence no atmosphere. This technique has identified LHS 3844 b (Kreidberg et al. 2019) and GJ 367 b (Zhang et al. 2024) as bare rocks — whilst the latter is dense enough to already expect a rock-iron composition, there is no mass measurement of the 1.3-$R_\oplus$ planet LHS 3844 b. However, atmospheric characterization – or ruling out an atmosphere — is and will only be available for a selection of a few planets, but not for the entire population of discovered planets.

4.2 Uncertainties on Mineral Physics Data and Their Effects on Interior Modelling

As the thermodynamic parameters in the EoS are determined from the fit to experimental values, along with the uncertainty on the fit there are two more sources of uncertainties that need to be considered. One is the operator error: A P-V-T equation of state fits up to six parameters with a dataset, which quite often cannot result in a unique solution when all the parameters are refined. As such, it is sometimes required to refine only a few parameters per fit, or to fix a parameter to a value obtained from the literature. Only an accurate and methodical test of all the possiblities will result in the operator chosing the best possible solution to their knowledge. This solution may be different from a refinement proposed by another author, who has chosen another formalism to best represent the data, and might be updated a few years later because a new dataset has been collected (Fig. 6a).

The second source of uncertainty is the experimental error. Data used to parametrize equations of state can come from high pressure and high temperature experiments and simulations. Depending on the techniques used for the experiments, the errors associated with the measurement of volume, pressure, and temperature during the experiment might be significant. In particular, diamond anvil cell experiments might carry a bigger uncertainty with respect to other experimental techniques (i.e. piston cylinder or multi anvil) at the experimental pressure and temperature due to the challenges in pressure calibration and the errors associated to temperature detection with spectroradiometry instead of using a thermocouple. It is the job of the researcher parametrizing the EoS to include those errors in the fit and assess how they affect the uncertainties on the parameterization. Uncertainties on DFT calculations are as well challenging to determine and they are dependent upon the specific packages that are used to calculate the intrinsic properties of matter among other (e.g., Mazdziarz 2024) and (Hakim et al. 2018) for an example of DFT application to exoplanets and the approach to uncertainties.

Applying EoS to super-Earths often necessitates extrapolating the density beyond the pressures and temperatures range covered by the data used to parametrize the EoS. This

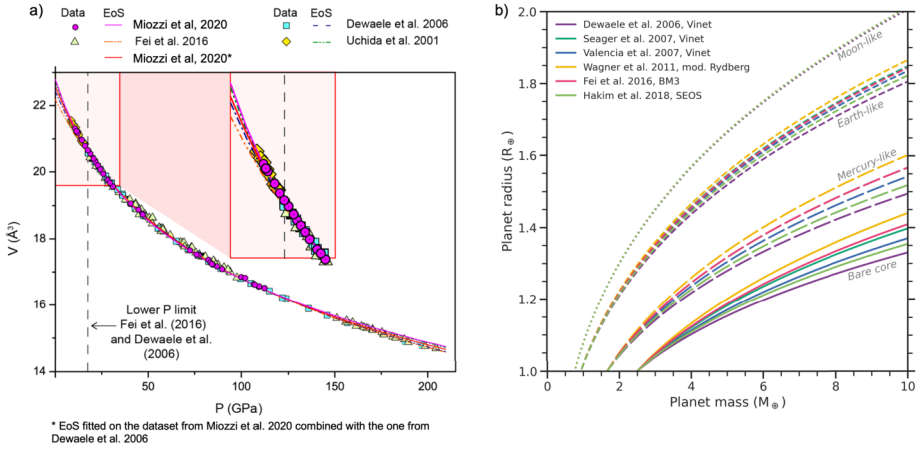

Fig. 6 a) Modified from Miozzi et al. (2020a). Collection of data representing the volume variation of iron with pressure at 300 K. Symbols are the experimental data, lines represent the best EoS parametrization for different authors. In the insert magnification of the lower pressure space, often challenging to investigate at high temperature. b) Variation of the calculated mass and radius, for different planets, induced by the use of a different Fe EoS, modified from Hakim et al. (2018)

can exacerbate the uncertainties coming from the fit of the thermodynamic parameters. In extreme cases when extrapolating to many Earth masses, EoS can assume non-physical behaviour, which is a mathematical artifact, but also an indication of the non-validity of the chosen EoS for this mass regime. Unterborn and Panero (2019) find that the impact of uncertainties is only minor when inferring the iron core size of rocky planets. However, a larger role is played by the choice of EoS itself, as shown in Hakim et al. (2018) and Fig. 6b. In addition, uncertainties in EoS parameters such as thermal expansivity can propagate into the determination of the adiabatic temperature profile, which may increase the error in the density calculations at high pressures. Fortunately, the effect of temperature is minor for rocky planets (see Sect. 3.2 and, e.g., Hakim et al. 2018).

The choice of interior EoS naturally assumes a specific mineralogy, as discussed throughout. Earth and the solar system (e.g., chondrites) are often used as baseline mineralogy. Meanwhile, theoretical studies have also explored how mineralogy would change for different bulk ratios of Fe, Mg and Si (e.g., Spaargaren et al. 2020; Guimond et al. 2023b, 2024). However, fewer studies have been dedicated to understanding the changes in mineralogy induced by a different content of volatiles along with the major forming elements. The discovery of 55 Cancri e and its initial conjecture as a carbon-rich planet (Madhusudhan et al. 2012) prompted some investigation into carbon-rich systems. Silicon carbide (SiC), for instance, was identified as one of the first compounds to condense in a C-rich environment; several studies have investigated its high-$P-T$ behaviour (e.g., Wilson and Militzer 2014; Nisr et al. 2017). The high abundances of sulphur and carbon in surface rocks of Mercury, indications of a very reducing oxygen fugacity (see also Sect. 5.4), have prompted a wealth of studies on carbon- and sulphur-rich systems (e.g., Zolotov 2011; Namur et al. 2016; Cartier and Wood 2019; Hakim et al. 2019). Oxygen fugacity is directly related to carbon- and sulphur-rich chemistry. For example, under reducing conditions, the solubility of sulphur in silicate melts increases dramatically, so that sulphur can exist in both the silicate and metallic phases in high concentrations (Kilburn and Wood 1997; Namur et al. 2016; Cartier and Wood 2019). Carbon under reducing conditions can be stable as graphite or carbides (Holloway et al. 1992; Holloway 1998). However, the results of these studies are not often integrated in the main databases for thermodynamic modelling,[3] as they did not focus on the thermo-physical properties of the stable mineralogical phases. An effort is required from the community to unveil and characterise phases and mineralogical assemblages that might become stable when both the bulk stellar composition and volatiles content is different from what observed in the solar system. It might turn out that the distribution of mineralogical phases and interior structures obtained for an Earth size planet in reality does not differ much from Earth — or it might differ a lot, presenting the chance to study new mineralogical assemblages and phases and implement them in available thermodynamic databases, and to analyze the potential diversity of planetary interiors in a more comprehensive manner.

5 Exoplanet Compositional Diversity and Constraints

5.1 Stellar Abundances

It is a working hypothesis that the relative abundances of rock-forming elements are roughly preserved during planet formation in the stellar nebula. Indeed, primitive chondrite meteorites and the solar photosphere show near-identical ratios of these elements (Palme et al.

[3] e.g., https://www.perplex.ethz.ch/perplex/datafiles/.

2014), used to inform estimates of the bulk silicate Earth composition (McDonough and Sun 1995); the same principle may be true for extrasolar systems. Some additional theoretical support comes from models of condensation in protoplanetary disks, which also reproduce Mg/Si and Fe/Si similar between disk and planet (Bond et al. 2010; Carter-Bond et al. 2012a,b; Moriarty et al. 2014; Thiabaud et al. 2015; Jorge et al. 2022).

Another, independent piece of information on planet rock-forming element composition is through elemental abundances in polluted white dwarf photospheres. The ultrahigh density and gravity of white dwarfs implies that any elements heavier than H and He in their photospheres must have likely come from a disintegrating object, possibly a planet, that fell onto it. Objects orbiting white dwarfs likely do not disintegrate onto the white dwarf all at once, and recovering the original elemental abundance and bulk composition of the original infalling object is made difficult by the uncertainty in the sinking timescales of various elements in the white dwarf's atmosphere (Buchan et al. 2022; Brouwers et al. 2023; Buchan et al. 2024). Nevertheless, comparisons of elemental abundances between polluted white dwarfs and main sequence stars provide weak observational support of a planet-star compositional connection. Photospheric Ca/Fe, Mg/Fe, and Si/Fe have been observed to match in two polluted white dwarfs their main-sequence binaries, which should be chemical twins of the white dwarf progenitor stars (Bonsor et al. 2021; Aguilera-Gómez et al. 2025). Further, Rogers et al. (2025) observe a correlation between polluted white dwarf photospheric Mg/Si ratios and the olivine/orthopyroxene ratios of circumstellar dust, supporting the idea that the mineralogy of (former) rocky planetary material turned to dust (see Sect. 5.2) can be inferred from polluted white dwarf photospheric elemental abundances. Trierweiler et al. (2023) compare the statistical distributions of various refractory and moderately-volatile abundance ratios between a sample of polluted white dwarfs and main-sequence FGKM stars, finding that the higher-metallicity stars show similar relative Fe abundances as the polluted white dwarf sample, though the spread of the latter is much wider. Testing the correlation of Fe content between that of the host star and that inferred from the planet bulk density is an active area of research (see Sect. 5.3).

If such a planet-star compositional correlation is real, then it would provide much-needed prior information on the interior structure of a planet. Earth is $\gtrsim$95% Fe, Mg, Si, and/or their oxides by mass (McDonough and Sun 1995; Wang et al. 2018). By loose analogy, knowing the relative Fe/Mg/Si make-up in the bulk planet will limit the range and proportions of possible materials (e.g., in the most simplified scenario, pure Fe-metal and pure $MgSiO_3$) and thus possible mass-radius curves that fit a bulk density observation (e.g., Dorn et al. 2015; Santos et al. 2015; Dorn et al. 2017b,a; Santos et al. 2017; Plotnykov and Valencia 2024) — an approach which has been used in practice even before a potentially-rocky exoplanet was detected (Dubois et al. 2002; Sotin et al. 2007). In an early study of how well these informed priors on bulk planet Fe/Mg/Si translate to interior structure and composition constraints, Dorn et al. (2015) showed that, with some simplifying assumptions and depending on the measurement precision, using stellar abundances allows a very good constraint on the radius of a pure-Fe core, and good constraints on the mantle Fe/Si ratio. This is because elemental abundance constraints strongly correlate core size with mantle composition.

This growing body of evidence is promising; nevertheless, it remains to be seen whether compositional diversity for rocky planets within individual systems can be observationally confirmed. Even with known stellar abundances, planets forming in different disk regions, especially around K-dwarfs, may have varying core mass fractions (Hatalova et al. 2025), including planets that are high Ca and Al contents (Dorn et al. 2019). This is indicated by a combination of planet formation simulations with equilibrium condensation models of protoplanetary disks. Correlations have been reported between inferred planet bulk Fe

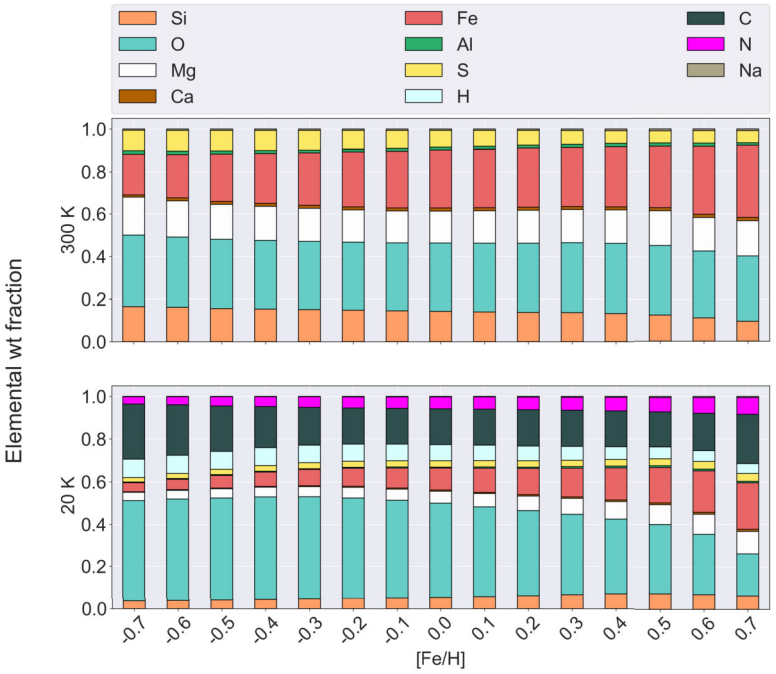

Fig. 7 Elemental weight fractions of planetary building blocks as a function of [Fe/H] at condensation temperatures of 20 K and 300 K. The data is derived from GALAH 3rd release and the Hypatia catalog

content and other properties, namely, the age of the system (Weeks et al. 2025) — and indeed the orbital periods of planets in our own Solar system (McDonough and Yoshizaki 2021) — indicating that multiple processes are at work to shape the bulk compositions of planets.

Bitsch and Battistini (2019) point out that most planet-forming simulations still rely on solar-like compositions, or on scaling the abundances of various elements using iron abundance trends. However, they show that stellar elemental abundances do not necessarily scale one-to-one with the (logarithmic) iron-to-hydrogen abundance (usually notated as [Fe/H] and normalised to the Sun). Figure 7 shows the elemental composition of planet-building blocks for different elements X as a function of [Fe/H] at two different condensation temperatures, based on data from the Hypatia catalog (for S, N, P) and the third release of the GALAH (Galactic Archeology with HERMES) survey (for Fe, C, Mg, O, Si, Al, Ca, Na).

5.2 Detailed Mantle Mineralogy from Thermodynamic Modelling

A common simplification in exoplanet interior modelling is that the mantle is a homogenous material with composition $MgSiO_3$ or $(Mg,Fe)SiO_3$. Meanwhile, xenolith samples from Earth's upper mantle and experimentally-constrained phase diagram modelling reveal a dozen different silicate mineral phases — including multiple polymorph minerals of the same chemical formula — which are thermodynamically stable depending on the local pressure and (less so) temperature. If such a detailed mineralogy were considered in interior structure models, one would require an EoS for each phase where it is stable, and combine them using the additive volume law (Eq. (1)). Further, although this article has somewhat

focussed on the structure of the solid interior of a planet in terms of only two "layers", the core and mantle, silicate phase transitions will define additional layers within the mantle (e.g., the postspinel transition separating Earth's upper and lower mantle). Layered structuring can alter patterns of mantle convection, potentially drastically (e.g., Tackley 1995; van den Berg et al. 2019), and transitions between mineral phases with differing volatile storage capacities may control how water and other volatiles are transported between interior and surface (e.g., Bercovici and Si 2003; Karato et al. 2013; Si et al. 2020; Guimond et al. 2023b).

As reviewed in Guimond et al. (2024), several studies have investigated how plausible variations in bulk oxide composition (see Sect. 5.1) affect the mantle mineralogy of known and hypothetical exoplanets (e.g., Hinkel and Unterborn 2018; Putirka and Rarick 2019; Wang et al. 2022a,b; Spaargaren et al. 2023; Guimond et al. 2023a,b). These studies estimate the proportions of mineral phases along a mantle geotherm, by way of Gibbs free energy minimisation routines (e.g., Connolly and Kerrick 1987; Ghiorso et al. 2002; Stixrude and Lithgow-Bertelloni 2024). A common result is that, if the observed variability of relative stellar abundances Mg/Si/Fe as well as Ca/Al (e.g., Hinkel et al. 2014) indeed represents the variability of exoplanet bulk oxide compositions $MgO/SiO_2/FeO/CaO/Al_2O_3$, then the vast majority of rocky planet mantle mineralogies would fall on the spectrum of dunite to orthopyroxenite, with upper mantle ratios of olivine to orthopyroxene strongly sensitive to the Mg/Si ratio. The predicted rarity of "exotic" mineralogies is a direct consequence of our Sun being typical in abundance ratios compared to the solar neighbourhood (see e.g., Spaargaren et al. 2023).

There are two important caveats to such results, both related to data paucity and already highlighted in Sect. 3.1 above. First, the thermodynamic data underlying Gibbs free energy minimisation models is poorly calibrated outside of Earth-like bulk compositions, and currently there is little understanding of the uncertainty due to extrapolating these compositions; e.g., to Mg/Si extremes. Second, the phase diagram of Mg-Fe-silicates at ultrahigh pressures (above several hundred GPa) is also poorly constrained, with our understanding limited mostly to molecular dynamics simulations (e.g., Umemoto et al. 2006, 2017; Umemoto and Wentzcovitch 2011) and a handful of static-compression experiments up to ~800 GPa (e.g., Coppari et al. 2013, 2021; Sakai et al. 2016). The unavoidably long timeframe of experimental work means that experimental constraints will often lag behind modelling developments. Knowing what exoplanet compositional diversity to expect in theory thus becomes immensely useful towards identifying which experiments should take priority; e.g., involving conditions expected on a large fraction of planets, or on particularly interesting or nearby targets.

Will variations in silicate mineralogy have a significant effect on observable masses and radii? Unterborn et al. (2016) systematically investigate the effect on mass-radius of the mantle Mg/Si, mantle Mg# = Mg/(Mg + Fe), and presence or absence of the postspinel transition, as well as the core light element composition, showing that reasonable variations of these parameters on a 1 $R_\oplus$ planet can lead to mass discrepancies of about 0.1 $M_\oplus$, 0.4 $M_\oplus$, 0.05 $M_\oplus$, and 0.2 $M_\oplus$ respectively. That is, the Mg# has the strongest effect on the mass-radius relationship, but its impact remains significantly smaller than the uncertainty in RV data. Overall, although the detailed composition of an exoplanet mantle will not be constrained given observational precision in most practical applications, mineralogy has a strong influence on the subsequent geodynamic evolution of a planet, as discussed in Sect. 6. Developing theory linking mantle compositions through to large-scale planetary consensequences is an important area of research.

5.3 Trends and Expectations in Rocky Planet Iron Contents

Regardless of detailed phase compositions, the most important component shaping the interior structure of a rocky planet is iron, because iron is heavy, is multivalent, and where it ends up in a planet is affected strongly by gravitational and redox differentiation (e.g., Wordsworth et al. 2018). The large spread in uncompressed bulk densities of the solar system terrestrial planets is attributed to an extent to the sizes of their metallic cores (e.g., McDonough and Yoshizaki 2021), composed of Fe and ∼15–20% alloyed elements. Between Mars and Mercury, core mass fractions (CMFs) range from ∼0.20–0.25 (Stähler et al. 2021; Khan et al. 2023) to ∼0.74 (Margot et al. 2018), posing an intriguing question as to what has caused these differences. In the solar system, Mercury is the clear anomaly, and there is no clear consensus on the origin of its large CMF: hypotheses include its mantle being stripped by early collisions (Cameron et al. 1988), or the planet simply forming with more iron overall (e.g., Weidenschilling 1978; Johansen and Dorn 2022; Mah and Bitsch 2023, see also Sect. 2.2). The fact that a planet's Fe content affects its bulk density so strongly is tied to Fe being the heaviest element expected in high cosmic abundance from stellar nucleosynthesis (Burbidge et al. 1957).

The first-order effect of iron mass fraction on bulk density means that it is somewhat tractable to define constraints on an exoplanet's iron mass fraction when thick volatile envelopes are unlikely. As discussed in the next section, bulk density is relatively insensitive to CMF specifically (except in the theoretical end-member scenario of a pure Fe core and an FeO-free mantle), but sensitive to iron mass fraction, so any inference of a CMF based on an interior structure model that presumes a pure iron core and an iron-free mantle should be interpreted as an iron mass fraction instead. In a sample of 32 exoplanets assumed to have no volatile envelopes, Adibekyan et al. (2021) estimate iron mass fractions across that sample ranging from ∼0 to ∼80%, implying an enormous range in compositional diversity.

If rocky exoplanet refractory compositions are inherited directly from their host stars (Sect. 5.1), we would expect a 1:1 correlation between these relative number abundances (e.g., Fe/Mg, Mg/Si) as measured in stars and the same relative abundances in bulk planets. It is acknowledged that protoplanetary disk processes, including accounting for the fact that rock-forming elements are not equally refractory ("devolatilisation"), should modify these ratios (e.g., Dauphas et al. (2015), Miyazaki and Korenaga (2017), Wang et al. (2019a), Adibekyan et al. (2024), see Guimond et al. 2024 for a recent review). Nevertheless, some amount of correlation between planet density and stellar iron content has been identified in the current sample, with Adibekyan et al. (2021) finding a 4:1 correlation, and more recently Brinkman et al. (2024) finding a correlation between 1:1 and 4:1 depending on (and highlighting the importance of) the choice of linear regression method. Both studies are therefore consistent with a planet-star compositional connection. Such statistical inferences remain challenging due to high observational uncertainty and small sample sizes, however; Schulze et al. (2021), for example, showed that only very discrepant planet/star iron contents could be resolved as such in the data.

5.4 Bulk Fe Redox States

The previous section has discussed how a planet's core mass fraction is not the same as its iron mass fraction. Whatever amount of iron a planet accretes, another crucial factor affecting its core size is the interior redox (e.g., the oxygen available to react) conditions that prevailed during formation of this core.

The importance of iron chemistry on interior structure motivates searching for the underlying distribution of core mass fractions of exoplanets. If we consider only iron and oxygen,

we might attempt to simplify the complicated, likely multi-stage process of core formation as the equilibrium between iron metal and iron oxide:

$$\underset{\text{metallic melt}}{\text{Fe}^0} + \frac{1}{2}\text{O}_2 \rightleftharpoons \underset{\text{silicate melt}}{\text{Fe}^{2+}\text{O}}\,, \tag{7}$$

where Fe and FeO are dissolved components in the metallic melt and the silicate melt, respectively. These immiscible melts would be equilibriating in the magma ocean of a young, very hot accreting planet, with gravity eventually causing the metal to settle as a planetary core. Equilibrium (7) shows that what redox state (0 or 2+) iron prefers depends on how easily an oxidising agent would be able to convert the metallic Fe into FeO: more-oxidising conditions would leave a smaller Fe core and an FeO-rich silicate mantle. This effective reactivity of O_2 is quantified via the oxygen fugacity, f_{O_2}. For example, in the approximation from Righter and Ghiorso (2012),

$$\Delta\text{IW} \approx -2\log\left(X_{\text{Fe}}/X_{\text{FeO}}\right), \tag{8}$$

X is the molar fraction in the metal or silicate phase, here in equilibrium with each other, and ΔIW is the dex difference in f_{O_2} with respect to equilbrium (7), known as the iron-wüstite or IW buffer for Fe and FeO as pure phases. In detail, f_{O_2} depends on the thermodynamic activity of all involved components (in (7), Fe and FeO) as well as pressure and temperature. Hence f_{O_2} is often used as a proxy for, though does not uniquely determine, the distribution of iron between its redox states (Frost 1991).

Because planetary cores are unlikely to be pure iron, their sizes will also depend on their light element composition. Detailed core compositions are difficult to constrain even for Earth, but are informed by measurements of metal-silicate partitioning coefficients for different elements, which dictate how much of an element enters a metallic phase (so ultimately the core) or a silicate phase (so ultimately the mantle) at chemical equilibrium. These coefficients depend strongly on f_{O_2} as well as temperature and pressure. At high pressures relevant for planetary core formation, many elements (but not H) become more siderophile as conditions become more oxidising (Suer et al. 2023). Core light element composition could affect core mass fraction for multiple reasons; e.g., via *(i)* adding material to the core, and *(ii)* decreasing the activity of metallic Fe and therefore the amount of FeO in equilibrium (7). Hence CMF will be a complicated function of f_{O_2}. Moreover, the presence of impurities depresses the melting point of iron (e.g., Morard et al. 2017), so f_{O_2} at core formation can also affect for how long the core is in a liquid state (and thus the choice of EOS in an interior structure model).

Running interior structure models, however, reveals that merely re-distributing iron between core and mantle at a fixed iron budget does not have a significant effect on planet bulk density. Rogers and Seager (2010), Noack and Lasbleis (2020) and Plotnykov and Valencia (2024) pointed out that increasing the iron content of a planet makes it similarly denser, regardless of whether the iron is dissolved as an oxide component in silicate solid solution, or whether it is in metallic form as a core to the planet. Figure 8 shows the insignificant effect on bulk density of changing Fe/FeO. Moreover, if Fe metal droplets cannot sink in a turbulent magma ocean, a core might never form (Lichtenberg 2021) despite the presence of this Fe. After all, iron redox chemistry in a real planet interior is much more complicated than equation (7), and is coupled with other elements. Therefore, if we wanted to define a bulk redox state of Fe in a planet, e.g., as the total mass of Fe versus Fe^{2+}, we could not easily extract this information from mass and radius measurements using interior structure models. Exoplanet bulk Fe redox states remain poorly constrained.

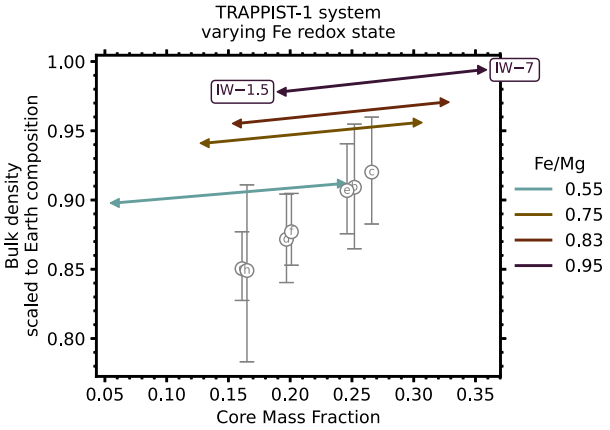

Fig. 8 The effect on bulk density of partitioning iron between the core and mantle. For each line of constant bulk-planet Fe/Mg (coloured lines), the FeO mantle fraction is calculated via a given ΔIW using (8), varied from −7 to −1.5, which results in a particular core mass fraction for each ΔIW and Fe/Mg. The resulting bulk density variations are much smaller than the observed bulk density uncertainties (grey errorbars) on the TRAPPIST-1 planets from Agol et al. (2021). Mantle EoS are from Stixrude and Lithgow-Bertelloni (2024) calculated using Perple_X and assuming an otherwise Earth-like composition. The core EoS is 100% solid hcp iron from Saxena and Eriksson (2015)

5.4.1 Oxygen Abundances from Polluted White Dwarfs

A series of studies (Doyle et al. 2019, 2020, 2023) sought to measure abundances of rock-forming elements Mg, Si, Ca, Al, Fe, and O in a growing sample of PWDs, and through comparison to solar system material, assess whether these extrasolar systems had similar relative oxygen abundances. Namely, these studies aim to find X_{FeO} in the polluting fragments, possible for systems with enough accounted O to form oxides with all the metals Mg, Si, Ca, Al, and Fe. Assuming that the accreted material in a PWD represented the bulk mantle composition, and assuming a value for the concentration X_{Fe} in a metallic phase in equilibrium with this mantle composition, then an estimate of ΔIW could be made using (8) (Righter and Ghiorso 2012). This value of ΔIW would indicate redox conditions during the parent body's differentiation, although it would not directly inform ΔIW in the upper mantle or at the surface of the body insofar as the local f_{O_2} is not buffered by Fe-metal here (e.g., Mojzsis 2022; Guimond et al. 2023a). Another source of difficulty in learning about bulk planet redox states from X_{FeO} in polluting fragments is that (8) is only meaningful when FeO coexists with a separate Fe-metal phase. However, many PWDs show an excess of oxygen, such that there is enough of it to bond to all Si, Mg, Al, Ca, and Fe, with some left over (e.g., Doyle et al. 2019; Brouwers et al. 2023). In this case, the application of (8) would presume that the parent body is differentiated, having formed long ago a Fe core – the coexisting Fe-metal phase needed to define bulk redox state – which would never be sampled in the detected 'mantle' fragment anyways. Another possibility is that the body never did differentiate. Then, for fragments showing excess oxygen, a bulk redox state in terms of ΔIW could not be strictly defined because there was never Fe-metal. Undifferentiated bodies may be difficult to distinguish from mantle-rich fragments in part of the PWD population (Buchan et al. 2024). In summary, inferring bulk redox states of parent planets using PWD oxygen abundances will require some caution, but is an intriguing avenue for population studies given enough samples (see Buchan et al. 2024).

5.5 Metal Core Composition and Light Element Content

Metallic cores are a result of metal-silicate differentiation taking place during planetary accretion. The main driver of the process is gravity, as Fe is denser than the surrounding silicates, but it also requires the presence of a melt and consequently temperatures sufficiently high to induce large scale melting (e.g., Lichtenberg et al. 2023, and references therein). As discussed in Sect. 5.4, the Fe/FeO budget of the forming planet and the chemical exchanges potentially happening during differentiation control the size and chemistry of the forming core. Elements will partition in the metal or in the silicates depending on their chemical affinity. Light elements, such as O, C, Si, S and H, are the prime candidates to enter the metal during differentiation. Their presence can affect the melting temperature (e.g., Morard et al. 2017, in the Fe-C system), volume and density (Miozzi et al. 2020b), and sound velocities (e.g., Badro et al. 2007). All of these factors are extremely relevant towards planets' large scale properties, from heat dissipation to the formation of an inner core and the driving of a geodynamo (for further discussion see Lourenço et al., this collection).

The inventory of light elements in the core is controlled by the initial bulk composition, the reactions taking place during formation and more importantly their solubility in the metal. The latter is not pivotal to assess as it depends on the pressure and temperature of the system. Hence one light element can be more prone to enter the metal at depth, while another might exsolve from the metal when a pressure/temperature threshold is passed (Hirose et al. 2021; Suer et al. 2023). For example, metal-silicate partitioning experiments for C have shown that carbon becomes more siderophile at high temperatures but less siderophile at high pressures (Dasgupta et al. 2013; Chi et al. 2014; Malavergne et al. 2019). Nevertheless, C is distributed roughly equally between the interior and the atmosphere of a planet (Suer et al. 2023). Hydrogen on the other hand becomes more siderophile as the pressure increases (Malavergne et al. 2019). The preferred incorporation of H and O in the core has also been shown by first principle simulations, making the core a potential large reservoir of water for rocky planets (Li et al. 2020; Yuan and Steinle-Neumann 2020). As a consequence, the carbon content of the core decreases with the mass of the planet, while the H content increases. The incorporation of N into the core depends both on the pressure and the oxygen fugacity, whereas N is only soluble in a magma ocean under very reduced conditions (Libourel et al. 2003; Grewal et al. 2019). Even so, the largest reservoir of N remains the atmosphere (Suer et al. 2023).

The effects of light elements on the thermal equation of state for solid iron have been widely investigated (e.g., Hirose et al. 2021; Litasov and Shatskiy 2016, and references therein). However, less is known about their effects on liquid metals, as the experimental field is still young. Exoplanet metal cores are often modelled as a pure iron sphere, and one single equation of state is used, although a few studies have considered variable core light element compositions, as a free parameter (Unterborn et al. 2016; Plotnykov and Valencia 2024; Haldemann et al. 2024, see also Sect. 5.2), or informed by solubility in metal (Luo et al. 2024). Any treatment of changes of state (e.g., liquid to solid) and their associated change of EoS will be complicated by the need to couple a thermal evolution model to the hydrostatic structure equations, given that the core is expected to lose heat over time, although solid-liquid phase changes might be considered statically (e.g., in Haldemann et al. 2024).

5.6 Devolatilization Trends

Proximity to the host star plays a critical role in planetary devolatilization, the process whereby the element abundances of planets would be to a degree sorted by condensation

temperature. Elements can be broadly characterised into two categories: Refractory elements, such as Al, Ca, Mg, Si, and Fe, form compounds with high condensation temperatures, typically above 1300 K. Volatile elements, including H, S, N, C, O, and the noble gases, have low condensation temperatures below 1100 K (e.g., Taylor 2001). While O and C are generally considered volatile, it should be noted here that they cannot be univocally classified as purely volatile or refractory, as they condense in both refractory and volatile compounds (Unterborn and Panero 2017; Wang et al. 2019b; Spaargaren et al. 2025). For example, Wang et al. (2019b), based on solar and Earth abundances, estimate that 20% of O is incorporated into refractory silicate mineral phases (see also Lodders 2003). Around carbon-enriched stars, carbon can be part of the first condensates (e.g., Madhusudhan et al. 2012).

Higher temperatures in the inner regions of a protoplanetary disk drive more intense volatile depletion, whereas cooler conditions at greater distances allow a larger fraction of volatiles to remain. Consequently, the radial distance and the associated thermal environment shape the observed volatility trends among planetary bodies.

Building on these general principles, Wang et al. (2019a) investigate the volatility of protosolar and terrestrial elemental abundances. They quantify devolatilization processes in a protoplanetary disk by comparing protosolar abundances with the composition of Earth using an improved combination of solar photospheric and CI chondrite abundances. This refined approach is crucial, as it allows for a more precise determination of the 'protosolar' composition, providing a robust baseline for comparison with terrestrial data. They derive a volatility trend, which indicates that elements with low condensation temperatures are more strongly depleted in Earth's composition compared to the protosolar material.

Outside the Solar System, it is not possible to rely on direct measurements. Consequently, complex models such as GGChem (Woitke et al. 2018) and FastChem (Stock et al. 2018) are used to simulate the condensation processes in a protoplanetary disk. The condensation curves shown in Fig. 9 are based on a much simpler model by Bitsch and Battistini (2019), providing a first approximation of a devolatilization trend in a protoplanetary disk around a star with [Fe/H] = 0.0 (i.e., solar; see Sect. 5.1). Here, elemental weight fractions of various condensed elements are plotted as a function of temperature within the disk. The lower

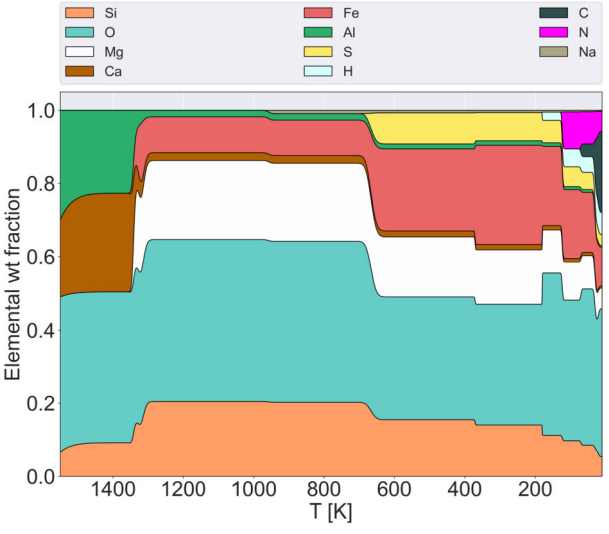

Fig. 9 Devolatilization trends for different elements as a function of temperature in a protoplanetary disk, assuming a Sun-like [Fe/H] = 0

the temperature–that is, the farther from the host star–the more volatile elements condense. Oxygen is an exception here, as oxygen-bearing compounds can already precipitate to form minerals at very high temperatures as discussed above.

5.7 Volatile Inventories

In contrast to gas giants, volatile elements like hydrogen, carbon, oxygen, and nitrogen are only a minor component in rocky planets. As discussed above, it is important to note that significant fractions of oxygen is in the refractory phase and therefore not counted as part of the volatile budget. Earth, the best studied rocky planet, contains on the order of 10 ppm N, 10^2 ppm of H, 10^3 ppm C, and ∼30% O (by mass, McDonough and Sun 1995; Wang et al. 2018). Taking into account that the oxygen abundance of the primitive mantle is estimated to be ∼44%, the volatile O budget of the Earth is on the order of 10^2 ppm (Palme and O'Neill 2005). While the exact composition of Mars is uncertain, there is both geophysical and cosmochemical evidence that Mars has a higher abundance of volatile elements than Earth (Khan et al. 2022). Despite their low abundances, volatile elements play an important role in shaping the planet in terms of it geological and biological evolution (e.g., Mikhail and Sverjensky 2014; Badro et al. 2014; Armstrong et al. 2015; Dehant et al. 2019; Krijt et al. 2023, see also Guimond et al., this collection).

Constraining the bulk volatile inventory of rocky planets is difficult as these elements are distributed over the core, mantle, surface and potential atmosphere of a planet (see Suer et al. 2023, for a recent review), on top of the fact that devolatilization (Sect. 5.7) is a poorly-known aspect of planet formation models. However, one important process determining the distribution of volatile elements in a planet is their solubility in an early magma ocean, and possible degassing from this magma ocean as it crystallises. Rapid formation, giant impacts, and radioactive decay cause rocky planets to melt and host (possibly multiple stages of) magma oceans during their early times (Elkins-Tanton 2012; Davies et al. 2020; Chao et al. 2021; Johansen et al. 2023). Another important process is the metal-silicate partitioning in this magma ocean, during core-mantle differentiation (Sect. 5.5).

Therefore, it can be important that interior structure models take the distribution of volatile elements into account, in particular for young or highly irradiated planets, as they have the potential to host magma oceans. Namely, the total radius of a rocky planet with a fully molten mantle and a given bulk water mass fraction can change by up to 25% depending on whether the water is only at the surface, or is also dissolved in the molten mantle and core (Dorn and Lichtenberg 2021; Luo et al. 2024). The interior water storage capacity of solid exoplanets, on the other hand, is much more limited (Iwamori 2007; Guimond et al. 2023b, see also Guimond et al., this collection). Therefore, the mantle outgasses a significant fraction of its water as it solidifies (e.g Gaillard et al. 2021, and Guimond et al., this collection).

The only direct way to detect volatile elements on a planet is to measure the composition of its atmosphere. However, there has been no clear detection of an atmosphere on a rocky exoplanet at the time of writing this article. Instead, the featureless spectra measured by JWST are consistent with both high mean molecular weight atmospheres composed of e.g., CH_4, CO_2 or H_2O, or with no atmospheres at all (Lustig-Yaeger et al. 2023; Zieba et al. 2023; Zhang et al. 2024; Alam et al. 2025). The best candidates to study the volatile component of rocky planets are underdense lava worlds, where dayside temperatures are hot enough to sustain a permanent magma ocean or pond, yet the stellar irradiation is not intense enough to strip any atmosphere of volatiles completely (e.g., Piette et al. 2023). One very promising example of such a lava-world is 55 Cancri e, which potentially hosts a CO- or CO_2-rich

atmosphere outgassed from an underlying magma ocean (Hu et al. 2024). The analysis of the atmosphere of 55 Cancri e, however, is complicated by the variability of the observed occultation depth and phase curve (Patel et al. 2024).

6 Implications for Exoplanet Geodynamics

Exoplanet astronomy is, by design, focussed mostly on the observable properties of a planet: mass, radius, and orbit, but also surface temperature and composition for atmosphere-less rocky bodies, or atmospheric chemistry otherwise. The hope to identify a planet with not only habitable surface conditions, but also signs of life, is one of the main drivers of the field, such that immense investments have been made into observational capabilities both in space and on ground (see also Lagage et al., this collection). For the most efficient use of future observatories, an optimal pre-selection of observational targets are needed, which led to the growing community focussing on geoscience aspects of exoplanets. After the first detection of rocky exoplanets almost two decades ago, theoretical studies (Valencia et al. 2006; Elkins-Tanton and Seager 2008; Noack et al. 2014; Dorn et al. 2018) quickly showed, that next to the planetary mass and radius, the interior structure is *the* main factor influencing the geodynamics of planets, and consequently their long-term evolutionary processes..

While several of the first theoretical studies of super-Earths took Earth as a benchmark for a rocky planet, and then explored how planetary processes such as plate tectonics, magnetic field strength, or volcanic activity would change if a model Earth were scaled up to higher planetary masses (Valencia et al. 2007; Van Heck and Tackley 2011; O'Neill et al. 2007; Noack and Breuer 2014; Noack et al. 2017; Kite et al. 2009; Driscoll and Olson 2011; Bonati et al. 2021), other studies showed that diverse interior structures also have geodynamic consequences (e.g., Elkins-Tanton and Seager 2008; Noack et al. 2014; Dorn et al. 2018; Lichtenberg 2021; Bonati et al. 2021; Baumeister et al. 2023). Incomplete differentiation of the core may both control and be controlled by interior redox conditions (see also Sect. 5.4). For example, inefficient formation of the core on massive super-Earths due to physical iron-metal entrainment would lead to a reducing mantle and hence a reducing atmosphere (Lichtenberg 2021), while inefficient core differentiation due to an oxidised formation scenario would conversely lead to an oxidising mantle and atmosphere (Elkins-Tanton and Seager 2008).

There are many reasons why interior structure and dynamics are linked; we provide a few more examples here. The existence of a magnetic field — shielding the surface and atmosphere from radiation — depends on core size, amongst other factors. A smaller core has been shown to favour a magnetic field on longer timescales due to less efficient cooling of the core through the thick, radiogenically heated mantle (Bonati et al. 2021). Thicker rocky mantles would permit volcanic outgassing over longer time scales (Noack et al. 2014), at least for low-mass rocky planets. The shallower pressure gradients permit deeper melt zones and facilitate melt extraction from deeper within the mantle. In addition, the cooling of thick mantles is less efficient, so that these planets retain their heat for a longer time. For more massive planets, volcanic activity depends on additional factors including the interior energy budget and the composition and compressibility of the melt, which may not be able to rise to the surface on massive rocky planets (Ohtani et al. 1995). Consideration of this melt buoyancy effect has lead to different predictions for volcanic activity on super-Earths (Kite et al. 2009; Noack et al. 2017). For example, Noack et al. (2017) find that volcanic activity becomes strongly limited at planet masses above 5 $M_\oplus$. Similarly, predictions of the likelihood of plate tectonics on super-Earth vary depending on other interior properties

such as heating rate or mantle composition (an in-depth literature overview can be found in Ballmer and Noack 2021). More recent studies have started to investigate the effects of variable mantle compositions (e.g. iron fraction as well as Mg/Si content) on mantle geodynamics (Dorn et al. 2018; Spaargaren et al. 2020): silicate composition influences mantle rheology and viscosity, melting temperatures, and other driving mantle properties. All of these studies require up-to-date interior structure models as a first step.

7 Conclusion and Perspectives

As seen in this review, determining the interior structure of rocky exoplanets is a complex multifaceted problem. Our interpretations of observations rely on indirect data alongside assumptions drawn from our knowledge of the Solar System. Many of the parameters that influence the interior remain unknown, difficult to measure, or potentially entirely unknowable. Compared to the wealth of information we have for the Solar System, the data available for exoplanets is limited and will likely remain so for the foreseeable future.

However, what exoplanet research may lack in terms of data diversity, it makes up for in scope: The growing population of detected, potentially rocky, exoplanets now far exceeds the small number of terrestrial planets in the Solar System. This allow for the first time the use of a statistical approach to planetary science testing the hypotheses about planet formation and evolution that the one data point of our Solar System can not provide. Furthermore, the discovery of planets with no analogue in the solar system present an opportunity to expand our knowledge and test different theories of formation.

We have entered the age of exoplanet atmosphere characterization owing to space telescopes such as the JWST and the upcoming ARIEL mission. These data can significantly contribute to deepen our understanding of exoplanets and their bulk and interior composition. Atmospheres on rocky planets are shaped by their interaction with the geodynamic processes taking place in the interiors. As atmosphere and interior are part of a single complex co-evolving system, the planets we observe today are the product of billions of years of evolution. To this end, one of the main scientific goals of the soon to be launched PLATO mission is to determine precise host star ages, and therefore the ages of their planets.

Understanding the interior-atmosphere link, and its time evolution, will be one of the major challenges in the upcoming years, but can lead to great rewards when coupled with the developments in observational techniques and instrumentation, improvements to numerical models, and upcoming space missions. These advancements will need to be combined with enhanced thermodynamic and modelling frameworks able to capture the evolution of the coupled interior-atmosphere system. Necessary to the development of such frameworks is the collection of high-quality datasets constraining the physicochemical properties of materials at high pressure and temperature. More efforts should be devoted to calibrate thermodynamic databases at extreme pressure and temperatures, and implement them with new mineralogical phases that might be uncommon on Earth but can exist for other formation conditions.

As our observational, experimental, and theoretical tools continue to improve, we move away from treating planets as just static spheres defined by bulk properties towards planets as dynamic evolving systems. Ultimately, determining the interior structure of rocky exoplanets provides the foundation on which all subsequent geophysical and atmospheric research builds upon. The main challenges ahead will involve linking diverse planetary processes, such as mantle convection, tectonics, volcanic outgassing, and the evolution of the atmosphere and surface. Perhaps most importantly, we should foster more collaboration among

the expert communities studying each of these areas. Interpreting exoplanet observations will require a holistic understanding of planetary systems that no single community possesses in isolation. Therefore, true progress in our understanding of rocky exoplanets will require a strong, multidisciplinary approach.

Acknowledgements The authors thank the two anonymous reviewers whose comments helped to improve the quality of this manuscript, as well as to the International Space Science Institute and the organizers for hosting and managing the workshop "The Geoscience of (Exo)planets: Going beyond habitability", from which this article originated. P.B., A.T., and L.N. are funded by the European Union (ERC, DIVERSE, 101087755). Views and opinions expressed are however those of the author(s) only and do not necessarily reflect those of the European Union or the European Research Council Executive Agency. Neither the European Union nor the granting authority can be held responsible for them. F.M. acknowledges support from the Carnegie Institution for Science and the Alfred P. Sloan Foundation under grant G202114194. CMG is supported by the UK STFC [grant number ST/W000903/1]. EB and AR acknowledge the financial support of the SNSF (grant number: 200021_197176 and 200020_215760). This work has been carried out within the framework of the NCCR PlanetS supported by the Swiss National Science Foundation under grants 51NF40_182901 and 51NF40_205606.

Funding Information Open Access funding enabled and organized by Projekt DEAL.

Declarations

Competing Interests The authors declare no competing interests.

References

Acuña L, Deleuil M, Mousis O, et al (2021) Characterisation of the hydrospheres of TRAPPIST-1 planets. Astron Astrophys 647:A53. https://doi.org/10.1051/0004-6361/202039885

Acuña L, Kreidberg L, Zhai M, et al (2024) GASTLI: an open-source coupled interior–atmosphere model to unveil gas-giant composition. Astron Astrophys 688:A60. https://doi.org/10.1051/0004-6361/202450559

Adibekyan V, Dorn C, Sousa SG, et al (2021) A compositional link between rocky exoplanets and their host stars. Science 374:330–332. https://doi.org/10.1126/science.abg8794

Adibekyan V, Deal M, Dorn C, et al (2024) Linking the primordial composition of planet building disks to the present-day composition of rocky exoplanets. Astron Astrophys 692:A67. https://doi.org/10.1051/0004-6361/202452193

Agol E, Dorn C, Grimm SL, et al (2021) Refining the transit-timing and photometric analysis of TRAPPIST-1: masses, radii, densities, dynamics, and ephemerides. Planet Sci J 2(1):1. https://doi.org/10.3847/PSJ/abd022

Aguichine A (2024) Mardigras: a visualization tool of theoretical mass–radius relations in the context of planetary science. Res Notes AAS 8(8):216. https://doi.org/10.3847/2515-5172/ad7506

Aguilera-Gómez C, Rogers LK, Bonsor A, et al (2025) Host star and exoplanet composition: polluted white dwarf reveals depletion of moderately refractory elements in planetary material. Astron Astrophys 693:A64. https://doi.org/10.1051/0004-6361/202451621

Akeson R, Armus L, Bachelet E, et al (2019) The Wide Field Infrared Survey Telescope: 100 Hubbles for the 2020s. arXiv e-prints. https://doi.org/10.48550/arXiv.1902.05569. arXiv:1902.05569

Alam MK, Gao P, Adams Redai J, et al (2025) JWST COMPASS: the first near- to mid-infrared transmission spectrum of the hot super-Earth l 168-9 b. Astron J 169(1):15. https://doi.org/10.3847/1538-3881/ad8eb5. arXiv:2411.03154 [astro-ph.EP]

Al'tshuler LV, Bakanova A (1969) Electronic structure and compressibility of metals at high pressures. Sov Phys Usp 11(5):678

Angel RJ (2000) Equations of state. Rev Mineral Geochem 41(1):35–59. https://doi.org/10.2138/rmg.2000.41.2

Angel RJ, Alvaro M, Nestola F (2018) 40 years of mineral elasticity: a critical review and a new parameterisation of equations of state for mantle olivines and diamond inclusions. Phys Chem Miner 45(2):95–113. https://doi.org/10.1007/s00269-017-0900-7

Armstrong LS, Hirschmann MM, Stanley BD, et al (2015) Speciation and solubility of reduced C-O-H-N volatiles in mafic melt: implications for volcanism, atmospheric evolution, and deep volatile cycles in the terrestrial planets. Geochim Cosmochim Acta 171:283–302. https://doi.org/10.1016/j.gca.2015.07.007

Badro J, Fiquet G, Guyot F, et al (2007) Effect of light elements on the sound velocities in solid iron: implications for the composition of Earth's core. Earth Planet Sci Lett 254(1–2):233–238

Badro J, Côté AS, Brodholt JP (2014) A seismologically consistent compositional model of Earth's core. Proc Natl Acad Sci USA 111(21):7542–7545. https://doi.org/10.1073/pnas.1316708111

Ballmer MD, Noack L (2021) The diversity of exoplanets: from interior dynamics to surface expressions. Elements 17(4):245–250

Baumeister P, Tosi N (2023) ExoMDN: rapid characterization of exoplanet interior structures with mixture density networks. Astron Astrophys 676:A106. https://doi.org/10.1051/0004-6361/202346216

Baumeister P, Padovan S, Tosi N, et al (2020) Machine-learning inference of the interior structure of low-mass exoplanets. Astrophys J 889(1):42. https://doi.org/10.3847/1538-4357/ab5d32

Baumeister P, Tosi N, Brachmann C, et al (2023) Redox state and interior structure control on the long-term habitability of stagnant-lid planets. Astron Astrophys 675:A122. https://doi.org/10.1051/0004-6361/202245791

Beaulieu JP, Bowles N, Coudé Du Foresto V, et al (2018) The ARIEL space mission. In: MacEwen HA, Lystrup M, Fazio GG, et al (eds) Space telescopes and instrumentation 2018: optical, infrared, and millimeter wave. SPIE, Austin, p 16. https://doi.org/10.1117/12.2311838

Benneke B, Roy PA, Coulombe LP, et al (2024) JWST reveals CH_4, CO_2, and H_2O in a metal-rich miscible atmosphere on a two-Earth-radius exoplanet. arXiv e-prints. https://doi.org/10.48550/ARXIV.2403.03325

Benz W, Slattery WL, Cameron AGW (1988) Collisional stripping of Mercury's mantle. Icarus 74(3):516–528. https://doi.org/10.1016/0019-1035(88)90118-2

Bercovici D, Si K (2003) Whole-mantle convection and the transition-zone water filter. Nature 425(6953):39–44. https://doi.org/10.1038/nature01918

Bitsch B, Battistini C (2019) Influence of sub- and super-solar metallicities on the composition of solid planetary building blocks. Astron Astrophys 633:A10. https://doi.org/10.1051/0004-6361/201936463

Bonati I, Lasbleis M, Noack L (2021) Structure and thermal evolution of exoplanetary cores. J Geophys Res Planets 126(5):e2020JE006724

Bond JC, O'Brien DP, Lauretta DS (2010) The compositional diversity of extrasolar terrestrial planets: I. In-situ simulations. Astrophys J 715(2):1050–1070. https://doi.org/10.1088/0004-637X/715/2/1050. arXiv:1004.0971

Bonomo AS, Zeng L, Damasso M, et al (2019) A giant impact as the likely origin of different twins in the Kepler-107 exoplanet system. Nat Astron 3:416–423. https://doi.org/10.1038/s41550-018-0684-9. arXiv:1902.01316 [astro-ph.EP]

Bonsor A, Jofré P, Shorttle O, et al (2021) Host-star and exoplanet compositions: a pilot study using a wide binary with a polluted white dwarf. Mon Not R Astron Soc 503(2):1877–1883. https://doi.org/10.1093/mnras/stab370

Borucki WJ, Koch D, Basri G, et al (2010) Kepler planet-detection mission: introduction and first results. Science 327(5968):977. https://doi.org/10.1126/science.1185402

Bradley PA, Loomis EN, Merritt EC, et al (2018) Experimental validation of thermodynamic mixture rules at extreme pressures and densities. Phys Plasmas 25(1):012710. https://doi.org/10.1063/1.5006200

Brinkman CL, Polanski AS, Huber D, et al (2024) Revisiting the relationship between rocky exoplanet and stellar compositions: reduced evidence for a super-Mercury population. Astron J 168(6):281. https://doi.org/10.3847/1538-3881/ad82eb. arXiv:2409.08361 [astro-ph.EP]

Brouwers MG, Buchan AM, Bonsor A, et al (2023) Asynchronous accretion can mimic diverse white dwarf pollutants II: water content. Mon Not R Astron Soc 519:2663–2679. https://doi.org/10.1093/mnras/stac3317

Buchan AM, Bonsor A, Shorttle O, et al (2022) Planets or asteroids? A geochemical method to constrain the masses of white dwarf pollutants. Mon Not R Astron Soc 510:3512–3530. https://doi.org/10.1093/mnras/stab3624
Buchan AM, Rogers LK, et al (2024) White dwarf constraints on geological processes at the population level. Mon Not R Astron Soc 532(2):2705–2723. https://doi.org/10.1093/mnras/stae1608
Burbidge EM, Burbidge GR, Fowler WA, et al (1957) Synthesis of the elements in stars. Rev Mod Phys 29(4):547–650. https://doi.org/10.1103/RevModPhys.29.547
Burn R, Mordasini C, Mishra L, et al (2024) A radius valley between migrated steam worlds and evaporated rocky cores. Nat Astron 8(4):463–471. https://doi.org/10.1038/s41550-023-02183-7
Cambioni S, Weiss BP, Asphaug E, et al (2025) Can metal-rich worlds form by giant impacts? Astron Astrophys 696:A174. https://doi.org/10.1051/0004-6361/202450128
Cameron AGW (1985) The partial volatilization of Mercury. Icarus 64(2):285–294. https://doi.org/10.1016/0019-1035(85)90091-0
Cameron AGW, Benz W, Fegley B Jr, et al (1988) The strange density of Mercury - theoretical considerations
Carrión-González Ó, García Muñoz A, Santos NC, et al (2021) Catalogue of exoplanets accessible in reflected starlight to the Nancy Grace Roman Space Telescope: population study and prospects for phase-curve measurements. Astron Astrophys 651:A7. https://doi.org/10.1051/0004-6361/202039993
Carter-Bond JC, O'Brien DP, Delgado Mena E, et al (2012a) Low Mg/Si planetary host stars and their Mg-depleted terrestrial planets. Astrophys J 747:L2. https://doi.org/10.1088/2041-8205/747/1/L2
Carter-Bond JC, O'Brien DP, Raymond SN (2012b) The compositional diversity of extrasolar terrestrial planets. II. Migration simulations. Astrophys J 760:44. https://doi.org/10.1088/0004-637X/760/1/44
Cartier C, Wood BJ (2019) The role of reducing conditions in building Mercury. Elements 15(1):39–45. https://doi.org/10.2138/gselements.15.1.39
Castro-González A, Demangeon ODS, Lillo-Box J, et al (2023) An unusually low-density super-Earth transiting the bright early-type M-dwarf GJ 1018 (TOI-244). Astron Astrophys 675:A52. https://doi.org/10.1051/0004-6361/202346550
Chao KH, deGraffenried R, Lach M, et al (2021) Lava worlds: from early Earth to exoplanets. Chem Erde 81(2):125735. https://doi.org/10.1016/j.chemer.2020.125735. arXiv:2012.07337 [astro-ph.EP]
Chen J, Kipping DM (2017) Probabilistic forecasting of the masses and radii of other worlds. Astrophys J 834(1):17. https://doi.org/10.3847/1538-4357/834/1/17. arXiv:1603.08614 [astro-ph]
Chi H, Dasgupta R, Duncan MS, et al (2014) Partitioning of carbon between Fe-rich alloy melt and silicate melt in a magma ocean - implications for the abundance and origin of volatiles in Earth, Mars, and the Moon. Geochim Cosmochim Acta 139:447–471. https://doi.org/10.1016/j.gca.2014.04.046
Connolly JAD, Kerrick DM (1987) An algorithm and computer program for calculating composition phase diagrams. Calphad 11(1):1–55. https://doi.org/10.1016/0364-5916(87)90018-6
Coppari F, Smith RF, Eggert JH, et al (2013) Experimental evidence for a phase transition in magnesium oxide at exoplanet pressures. Nat Geosci 6(11):926–929. https://doi.org/10.1038/ngeo1948
Coppari F, Smith RF, Wang J, et al (2021) Implications of the iron oxide phase transition on the interiors of rocky exoplanets. Nat Geosci 14:121–126. https://doi.org/10.1038/s41561-020-00684-y
Dasgupta R, Chi H, Shimizu N, et al (2013) Carbon solution and partitioning between metallic and silicate melts in a shallow magma ocean: implications for the origin and distribution of terrestrial carbon. Geochim Cosmochim Acta 102:191–212. https://doi.org/10.1016/j.gca.2012.10.011
Dauphas N, Poitrasson F, Burkhardt C, et al (2015) Planetary and meteoritic Mg/Si and δ30Si variations inherited from solar nebula chemistry. Earth Planet Sci Lett 427:236–248. https://doi.org/10.1016/j.epsl.2015.07.008
Davies EJ, Carter PJ, Root S, et al (2020) Silicate melting and vaporization during rocky planet formation. J Geophys Res Planets 125(2):e06227. https://doi.org/10.1029/2019JE006227. arXiv:2002.00998 [astro-ph.EP]
Dehant V, Debaille V, Dobos V, et al (2019) Geoscience for understanding habitability in the Solar System and beyond. Space Sci Rev 215(6):42. https://doi.org/10.1007/s11214-019-0608-8. arXiv:1909.00362 [astro-ph.EP]
Demory BO, Gillon M, Deming D, et al (2011) Detection of a transit of the super-Earth 55 Cancri e with warm Spitzer. Astron Astrophys 533:A114. https://doi.org/10.1051/0004-6361/201117178. arXiv:1105.0415 [astro-ph.EP]
Dorn C, Lichtenberg T (2021) Hidden water in magma ocean exoplanets. Astrophys J 922(1):L4. https://doi.org/10.3847/2041-8213/ac33af. arXiv:2110.15069 [astro-ph.EP]
Dorn C, Khan A, Heng K, et al (2015) Can we constrain interior structure of rocky exoplanets from mass and radius measurements? Astron Astrophys 577:A83. https://doi.org/10.1051/0004-6361/201424915. arXiv:1502.03605
Dorn C, Hinkel NR, Venturini J (2017a) Bayesian analysis of interiors of HD 219134b, Kepler-10b, Kepler-93b, CoRoT-7b, 55 Cnc e, and HD 97658b using stellar abundance proxies. Astron Astrophys 597:A38. https://doi.org/10.1051/0004-6361/201628749

Dorn C, Venturini J, Khan A, et al (2017b) A generalized Bayesian inference method for constraining the interiors of super Earths and sub-Neptunes. Astron Astrophys 597:A37. https://doi.org/10.1051/0004-6361/201628708. arXiv:1609.03908

Dorn C, Noack L, Rozel A (2018) Outgassing on stagnant-lid super-Earths. Astron Astrophys 614:A18

Dorn C, Harrison JHD, Bonsor A, et al (2019) A new class of super-Earths formed from high-temperature condensates: HD219134 b, 55 Cnc e, WASP-47 e. Mon Not R Astron Soc 484:712–727. https://doi.org/10.1093/mnras/sty3435

Dou J, Carter PJ, Leinhardt ZM (2024) Formation of super-Mercuries via giant impacts. Mon Not R Astron Soc 529(3):2577–2594. https://doi.org/10.1093/mnras/stae644. arXiv:2403.03831 [astro-ph.EP]

Doyle AE, Young ED, Klein B, et al (2019) Oxygen fugacities of extrasolar rocks: evidence for an Earth-like geochemistry of exoplanets. Science 366(6463):356–359. https://doi.org/10.1126/science.aax3901

Doyle AE, Klein B, Schlichting HE, et al (2020) Where are the extrasolar Mercuries? Astrophys J 901(1):10. https://doi.org/10.3847/1538-4357/abad9a

Doyle AE, Klein BL, Dufour P, et al (2023) New chondritic bodies identified in eight oxygen-bearing white dwarfs. Astrophys J 950:93. https://doi.org/10.3847/1538-4357/acbd44

Driscoll P, Olson P (2011) Optimal dynamos in the cores of terrestrial exoplanets: magnetic field generation and detectability. Icarus 213(1):12–23

Dubois V, Mocquet A, Sotin C (2002) Effect of the chemistry of the stellar nebula on the relationship between mass and radius of silicate and metal rich exoplanets. In: EGS general assembly conference abstracts, p 4010

Ducrot E, Lagage PO, Min M, et al (2025) Combined analysis of the 12.8 and 15 μm JWST/MIRI eclipse observations of TRAPPIST-1 b. Nat Astron 9:358–369. https://doi.org/10.1038/s41550-024-02428-z

Duffy TS, Smith RF (2019) Ultra-high pressure dynamic compression of geological materials. Front Earth Sci 7:23. https://doi.org/10.3389/feart.2019.00023

Duffy T, Madhusudhan N, Lee KKM (2015) 2.07 - mineralogy of super-Earth planets. In: Schubert G (ed) Treatise on geophysics, 2nd edn. Elsevier, Oxford, pp 149–178. https://doi.org/10.1016/B978-0-444-53802-4.00053-1

Dziewonski AM, Anderson DL (1981) Preliminary reference Earth model. Phys Earth Planet Inter 25(4):297–356

Egger JA, Osborn HP, Kubyshkina D, et al (2024) Unveiling the internal structure and formation history of the three planets transiting HIP 29442 (TOI-469) with CHEOPS. Astron Astrophys 688:A223. https://doi.org/10.1051/0004-6361/202450472

Elkins-Tanton LT (2012) Magma oceans in the inner Solar System. Annu Rev Earth Planet Sci 40(1):113–139. https://doi.org/10.1146/annurev-earth-042711-105503

Elkins-Tanton LT, Seager S (2008) Coreless terrestrial exoplanets. Astrophys J 688(1):628

Fei Y (1995) Thermal expansion. In: Ahrens TJ (ed) Mineral physics and crystallography: a handbook of physical constants. American Geophysical Union, Washington, DC, pp 29–44. https://doi.org/10.1029/RF002p0029

Fei Y, Tracy SJ (2025) High pressure and temperature experiments. In: Anbar A, Weis D (eds) Treatise on geochemistry, 3rd edn. Elsevier, Amsterdam, pp 415–437. https://doi.org/10.1016/B978-0-323-99762-1.00085-1

Foley BJ, Houser C, Noack L, et al (2020) The heat budget of rocky planets. In: Tasker EJ, Unterborn C, Laneuville M, et al (eds) Planetary diversity. IOP Publishing, Bristol, pp 4–1–4–60. https://doi.org/10.1088/2514-3433/abb4d9ch4

Francesco A, Mario D (2022) pyExoRaMa: an interactive tool to investigate the radius-mass diagram for exoplanets. Zenodo. https://doi.org/10.5281/ZENODO.5899601

Frost BR (1991) Introduction to oxygen fugacity and its petrologic importance. Rev Mineral Geochem 25(1):1–9

Fulton BJ, Petigura EA (2018) The California-Kepler survey. VII. Precise planet radii leveraging Gaia DR2 reveal the stellar mass dependence of the planet radius gap. Astron J 156:264

Fulton BJ, Petigura EA, Howard AW, et al (2017) The California-Kepler survey. III. A gap in the radius distribution of small planets. Astron J 154(3):109. https://doi.org/10.3847/1538-3881/aa80eb. arXiv:1703.10375

Gaia Collaboration (2021) Gaia early data release 3: summary of the contents and survey properties. Astron Astrophys 649:A1. https://doi.org/10.1051/0004-6361/202039657

Gaidos E, Conrad CP, Manga M, et al (2010) Thermodynamic limits on magnetodynamos in rocky exoplanets. Astrophys J 718(2):596–609. https://doi.org/10.1088/0004-637X/718/2/596

Gaillard F, Bouhifd MA, Füri E, et al (2021) The diverse planetary ingassing/outgassing paths produced over billions of years of magmatic activity. Space Sci Rev 217(1):22. https://doi.org/10.1007/s11214-021-00802-1

Gardner JP, Mather JC, Clampin M, et al (2006) The James Webb Space Telescope. Space Sci Rev 123(4):485–606. https://doi.org/10.1007/s11214-006-8315-7. arXiv:astro-ph/0606175 [astro-ph]
Ghiorso MS, Hirschmann MM, Reiners PW, et al (2002) The pMELTS: a revision of MELTS for improved calculation of phase relations and major element partitioning related to partial melting of the mantle to 3 GPa. Geochem Geophys Geosyst 3(5):1–35. https://doi.org/10.1029/2001GC000217
Gillon M, Jehin E, Lederer SM, et al (2016) Temperate Earth-sized planets transiting a nearby ultracool dwarf star. Nature 533:221–224
Gillon M, Triaud AHMJ, Demory BO, et al (2017) Seven temperate terrestrial planets around the nearby ultracool dwarf star TRAPPIST-1. Nature 542:456–460
Gomez Casajus L, Zannoni M, Modenini D, et al (2021) Updated Europa gravity field and interior structure from a reanalysis of Galileo tracking data. Icarus 358:114187. https://doi.org/10.1016/j.icarus.2020.114187
Greene TP, Bell TJ, Ducrot E, et al (2023) Thermal emission from the Earth-sized exoplanet TRAPPIST-1 b using JWST. Nature 618(7963):39–42
Grewal DS, Dasgupta R, Holmes AK, et al (2019) The fate of nitrogen during core-mantle separation on Earth. Geochim Cosmochim Acta 251:87–115. https://doi.org/10.1016/j.gca.2019.02.009
Guimond CM, Shorttle O, Jordan S, et al (2023a) A mineralogical reason why all exoplanets cannot be equally oxidizing. Mon Not R Astron Soc 525(3):3703–3717. https://doi.org/10.1093/mnras/stad2486
Guimond CM, Shorttle O, Rudge JF (2023b) Mantle mineralogy limits to rocky planet water inventories. Mon Not R Astron Soc 521(2):2535–2552. https://doi.org/10.1093/mnras/stad148
Guimond CM, Wang H, Seidler F, et al (2024) From stars to diverse mantles, melts, crusts and atmospheres of rocky exoplanets. Rev Mineral Geochem 90(1):259–300. https://doi.org/10.2138/rmg.2024.90.08
Hakim K, Rivolidini A, Van Hoolst T, et al (2018) A new ab initio equation of state of hcp-Fe and its implication on the interior structure and mass-radius relations of rocky super-Earths. Icarus 313:61–78. https://doi.org/10.1016/j.icarus.2018.05.005
Hakim K, Van Den Berg A, Vazan A, et al (2019) Thermal evolution of rocky exoplanets with a graphite outer shell. Astron Astrophys 630:A152. https://doi.org/10.1051/0004-6361/201935714
Haldemann J, Ksoll V, Walter D, et al (2023) Exoplanet characterization using conditional invertible neural networks. Astron Astrophys 672:A180. https://doi.org/10.1051/0004-6361/202243230
Haldemann J, Dorn C, Venturini J, et al (2024) BICEPS: an improved characterization model for low- and intermediate-mass exoplanets. Astron Astrophys 681:A96. https://doi.org/10.1051/0004-6361/202346965
Hasegawa A, Ohta K, Yagi T, et al (2024) Inversion of the temperature dependence of thermal conductivity of hcp iron under high pressure. Sci Rep 14(1):23582
Hatalova P, Brodholt J, Brasser R, et al (2025) The compositional diversity of rocky exoplanets around k-dwarf stars. Astron Astrophys 694:A303
Hinkel NR, Unterborn CT (2018) The star–planet connection. I. Using stellar composition to observationally constrain planetary mineralogy for the 10 closest stars. Astrophys J 853(1):83. https://doi.org/10.3847/1538-4357/aaa5b4
Hinkel NR, Timmes FX, Young PA, et al (2014) Stellar abundances in the solar neighborhood: the hypatia catalog. Astron J 148:54. https://doi.org/10.1088/0004-6256/148/3/54
Hirose K, Wood B, Vočadlo L (2021) Light elements in the Earth's core. Nat Rev, Earth Environ 2(9):645–658
Holloway JR (1998) Graphite-melt equilibria during mantle melting: constraints on CO_2 in MORB magmas and the carbon content of the mantle. Chem Geol 147(1–2):89–97. https://doi.org/10.1016/S0009-2541(97)00174-5
Holloway JR, Pan V, Gudmundsson G (1992) High-pressure fluid-absent melting experiments in the presence of graphite: oxygen fugacity, ferric/ferrous ratio and dissolved CO_2. Eur J Mineral 4(1):105–114. https://doi.org/10.1127/ejm/4/1/0105
Hu R, Bello-Arufe A, Zhang M, et al (2024) A secondary atmosphere on the rocky exoplanet 55 Cancri e. Nature 630(8017):609–612. https://doi.org/10.1038/s41586-024-07432-x. arXiv:2405.04744 [astro-ph.EP]
Huang C, Rice DR, Steffen JH (2022) MAGRATHEA: an open-source spherical symmetric planet interior structure code. Mon Not R Astron Soc. https://doi.org/10.1093/mnras/stac1133
Hubbard W, Marley MS (1989) Optimized Jupiter, Saturn, and Uranus interior models. Icarus 78(1):102–118. https://doi.org/10.1016/0019-1035(89)90072-9
Iwamori H (2007) Transportation of H_2O beneath the Japan arcs and its implications for global water circulation. Chem Geol 239(3–4):182–198
Johansen A, Dorn C (2022) Nucleation and growth of iron pebbles explains the formation of iron-rich planets akin to Mercury. Astron Astrophys 662:A19. https://doi.org/10.1051/0004-6361/202243480

Johansen A, Ronnet T, Schiller M, et al (2023) Anatomy of rocky planets formed by rapid pebble accretion. II. Differentiation by accretion energy and thermal blanketing. Astron Astrophys 671:A75. https://doi.org/10.1051/0004-6361/202142142. arXiv:2207.09804 [astro-ph.EP]

Jontof-Hutter D (2019) The compositional diversity of low-mass exoplanets. Annu Rev Earth Planet Sci 47(1):141–171

Jorge DM, Kamp IEE, Waters LBFM, et al (2022) Forming planets around stars with non-solar elemental composition. Astron Astrophys 660:A85. https://doi.org/10.1051/0004-6361/202142738

Kanodia S, Wolfgang A, Stefansson GK, et al (2019) Mass–radius relationship for M dwarf exoplanets: comparing nonparametric and parametric methods. Astrophys J 882(1):38. https://doi.org/10.3847/1538-4357/ab334c

Karato SI, Bercovici D, Leahy G, et al (2013) The transition-zone water filter model for global material circulation: where do we stand? In: Jacobsen SD, Van Der Lee S (eds) Earth's deep water cycle. Geophysical monograph series. American Geophysical Union, Washington, DC, pp 289–313. https://doi.org/10.1029/168GM22

Katz RF, Spiegelman M, Langmuir CH (2003) A new parameterization of hydrous mantle melting. Geochem Geophys Geosyst 4(9):1073. https://doi.org/10.1029/2002GC000433

Khan A, Sossi PA, Liebske C, et al (2022) Geophysical and cosmochemical evidence for a volatile-rich Mars. Earth Planet Sci Lett 578:117330. https://doi.org/10.1016/j.epsl.2021.117330

Khan A, Huang D, Durán C, et al (2023) Evidence for a liquid silicate layer atop the Martian core. Nature 622(7984):718–723. https://doi.org/10.1038/s41586-023-06586-4

Kilburn M, Wood B (1997) Metal–silicate partitioning and the incompatibility of S and Si during core formation. Earth Planet Sci Lett 152(1–4):139–148. https://doi.org/10.1016/S0012-821X(97)00125-8

Kite ES, Manga M, Gaidos E (2009) Geodynamics and rate of volcanism on massive Earth-like planets. Astrophys J 700(2):1732

Konôpková Z, McWilliams RS, Gómez-Pérez N, et al (2016) Direct measurement of thermal conductivity in solid iron at planetary core conditions. Nature 534(7605):99–101

Kreidberg L, Koll DDB, Morley C, et al (2019) Absence of a thick atmosphere on the terrestrial exoplanet LHS 3844b. Nature 573(7772):87–90. https://doi.org/10.1038/s41586-019-1497-4

Krijt S, Kama M, McClure M, et al (2023) Chemical habitability: supply and retention of life's essential elements during planet formation. In: Inutsuka S, et al (eds) Protostars and planets VII, Astronomical Society of the Pacific, San Francisco, p 1031. https://doi.org/10.48550/arXiv.2203.10056. arXiv:2203.10056

Kroll H, Kirfel A, Heinemann R (2012) Volume thermal expansion and related thermophysical parameters in the Mg, Fe olivine solid-solution series. Eur J Mineral 26(5):607–621. https://doi.org/10.1127/0935-1221/2014/0026-2398

Lam KWF, Csizmadia S, Astudillo-Defru N, et al (2021) GJ 367b: a dense, ultrashort-period sub-Earth planet transiting a nearby red dwarf star. Science 374(6572):1271–1275. https://doi.org/10.1126/science.aay3253. arXiv:2112.01309 [astro-ph.EP]

Li Y, Vočadlo L, Sun T, et al (2020) The Earth's core as a reservoir of water. Nat Geosci 13(6):453–458. https://doi.org/10.1038/s41561-020-0578-1

Libourel G, Marty B, Humbert F (2003) Nitrogen solubility in basaltic melt. Part I. Effect of oxygen fugacity. Geochim Cosmochim Acta 67(21):4123–4135. https://doi.org/10.1016/S0016-7037(03)00259-X

Lichtenberg T (2021) Redox hysteresis of super-Earth exoplanets from magma ocean circulation. Astrophys J Lett 914:L4. https://doi.org/10.3847/2041-8213/ac0146

Lichtenberg T, Schaefer LK, Nakajima M, et al (2023) Geophysical evolution during rocky planet formation. In: Inutsuka S, et al (eds) Protostars and planets VII. Astronomical Society of the Pacific, San Francisco, pp 907–946. https://doi.org/10.48550/arXiv.2203.10056

Lim O, Benneke B, Doyon R, et al (2023) Atmospheric reconnaissance of TRAPPIST-1 b with JWST/NIRISS: evidence for strong stellar contamination in the transmission spectra. Astrophys J 955(1):L22

Litasov KD, Shatskiy AF (2016) Composition of the Earth's core: a review. Russ Geol Geophys 57(1):22–46

Liu Z, Ni D (2023) Quantitative correlation of refractory elemental abundances between rocky exoplanets and their host stars. Astron Astrophys 674:A137. https://doi.org/10.1051/0004-6361/202245387

Lodders K (2003) Solar System abundances and condensation temperatures of the elements. Astrophys J 591(2):1220–1247. https://doi.org/10.1086/375492

Luo H, Dorn C, Deng J (2024) The interior as the dominant water reservoir in super-Earths and sub-Neptunes. Nat Astron 8:1399–1407. https://doi.org/10.1038/s41550-024-02347-z. arXiv:2401.16394 [astro-ph.EP]

Lustig-Yaeger J, Fu G, May EM, et al (2023) A JWST transmission spectrum of the nearby Earth-sized exoplanet LHS 475 b. Nat Astron 7:1317–1328. https://doi.org/10.1038/s41550-023-02064-z. arXiv:2301.04191 [astro-ph.EP]

Madhusudhan N, Lee KKM, Mousis O (2012) A possible carbon-rich interior in super-Earth 55 Cancri e. Astrophys J 759(2):L40. https://doi.org/10.1088/2041-8205/759/2/L40
Mah J, Bitsch B (2023) Forming super-Mercuries: role of stellar abundances. Astron Astrophys 673:A17. https://doi.org/10.1051/0004-6361/202346021
Malavergne V, Bureau H, Raepsaet C, et al (2019) Experimental constraints on the fate of H and C during planetary core-mantle differentiation. Implications for the Earth. Icarus 321:473–485. https://doi.org/10.1016/j.icarus.2018.11.027
Marcus RA, Sasselov D, Hernquist L, et al (2010) Minimum radii of super-Earths: constraints from giant impacts. Astrophys J 712(1):L73–L76. https://doi.org/10.1088/2041-8205/712/1/L73. arXiv:1003.0451 [astro-ph.EP]
Margot JL, Hauck SA, Mazarico E, et al (2018) Mercury's internal structure. In: Solomon SC, et al (eds) Mercury: the view after MESSENGER. Cambridge University Press, Cambridge, pp 85–113. https://doi.org/10.1017/9781316650684.005. arXiv:1806.02024
Mayor M, Marmier M, Lovis C, et al (2011) The HARPS search for southern extra-solar planets XXXIV. Occurrence, mass distribution and orbital properties of super-Earths and Neptune-mass planets. arXiv e-prints. https://doi.org/10.48550/arXiv.1109.2497. arXiv:1109.2497 [astro-ph.EP]
Mazdziarz M (2024) Uncertainty of dft calculated mechanical and structural properties of solids due to incompatibility of pseudopotentials and exchange–correlation functionals. J Chem Theory Comput 20(21):9734–9740. https://doi.org/10.1021/acs.jctc.4c01036
McDonough WF, Sun S-S (1995) The composition of the Earth. Chem Geol 120(3):223–253. https://doi.org/10.1016/0009-2541(94)00140-4
McDonough WF, Yoshizaki T (2021) Terrestrial planet compositions controlled by accretion disk magnetic field. Prog Earth Planet Sci 8:39. https://doi.org/10.1186/s40645-021-00429-4
Mikhail S, Sverjensky DA (2014) Nitrogen speciation in upper mantle fluids and the origin of Earth's nitrogen-rich atmosphere. Nat Geosci 7(11):816–819. https://doi.org/10.1038/ngeo2271
Miozzi F, Matas J, Guignot N, et al (2020a) A new reference for the thermal equation of state of iron. Minerals 10(2):100
Miozzi F, Morard G, Antonangeli D, et al (2020b) Eutectic melting of Fe-3 at% Si-4 at% C up to 200 GPa and implications for the Earth's core. Earth Planet Sci Lett 544:116382
Miyazaki Y, Korenaga J (2017) Effects of chemistry on vertical dust motion in early protoplanetary disks. Astrophys J 849(1):41. https://doi.org/10.3847/1538-4357/aa8cd1
Mojzsis SJ (2022) Geoastronomy: rocky planets as the Lavoisier–Lomonosov bridge from the non-living to the living world. In: Fiore M (ed) Prebiotic chemistry and life's origins. The Royal Society of Chemistry, pp 21–76. https://doi.org/10.1039/9781839164798-00021
Morard G, Andrault D, Antonangeli D, et al (2017) Fe–FeO and Fe–Fe_3C melting relations at Earth's core–mantle boundary conditions: implications for a volatile-rich or oxygen-rich core. Earth Planet Sci Lett 473:94–103
Moriarty J, Madhusudhan N, Fischer D (2014) Chemistry in an evolving protoplanetary disk: effects on terrestrial planet composition. Astrophys J 787:81. https://doi.org/10.1088/0004-637X/787/1/81
Murgas F, Pallé E, Orell-Miquel J, et al (2024) Wolf 327b: a new member of the pack of ultra-short-period super-Earths around M dwarfs. Astron Astrophys 684:A83. https://doi.org/10.1051/0004-6361/202348813. arXiv:2401.12150 [astro-ph.EP]
Myhill R, Cottaar S, Heister T, et al (2023) BurnMan – a Python toolkit for planetary geophysics, geochemistry and thermodynamics. J Open Source Softw 8(87):5389. https://doi.org/10.21105/joss.05389
Namur O, Charlier B, Holtz F, et al (2016) Sulfur solubility in reduced mafic silicate melts: implications for the speciation and distribution of sulfur on Mercury. Earth Planet Sci Lett 448:102–114. https://doi.org/10.1016/j.epsl.2016.05.024
National Academies of Sciences, Engineering, and Medicine (2023) Pathways to discovery in astronomy and astrophysics for the 2020s. The National Academies Press, Washington. https://doi.org/10.17226/26141
Nettelmann N, Holst B, Kietzmann A, et al (2008) Ab initio equation of state data for hydrogen, helium, and water and the internal structure of Jupiter. Astrophys J 683(2):1217–1228. https://doi.org/10.1086/589806
Nisr C, Meng Y, MacDowell A, et al (2017) Thermal expansion of sic at high pressure-temperature and implications for thermal convection in the deep interiors of carbide exoplanets. J Geophys Res Planets 122(1):124–133
Nixon MC, Madhusudhan N (2021) How deep is the ocean? Exploring the phase structure of water-rich sub-Neptunes. Mon Not R Astron Soc 505(3):3414–3432. https://doi.org/10.1093/mnras/stab1500
Noack L, Breuer D (2014) Plate tectonics on rocky exoplanets: influence of initial conditions and mantle rheology. Planet Space Sci 98:41–49
Noack L, Lasbleis M (2020) Parameterisations of interior properties of rocky planets: an investigation of planets with Earth-like compositions but variable iron content. Astron Astrophys 638:A129. https://doi.org/10.1051/0004-6361/202037723

Noack L, Godolt M, von Paris P, et al (2014) Can the interior structure influence the habitability of a rocky planet? Planet Space Sci 98:14–29
Noack L, Höning D, Rivoldini A, et al (2016) Water-rich planets: how habitable is a water layer deeper than on Earth? Icarus 277:215–236
Noack L, Rivoldini A, Van Hoolst T (2017) Volcanism and outgassing of stagnant-lid planets: implications for the habitable zone. Phys Earth Planet Inter 269:40–57
Ohta K, Kuwayama Y, Hirose K, et al (2016) Experimental determination of the electrical resistivity of iron at Earth's core conditions. Nature 534(7605):95–98
Ohtani E, Nagata Y, Suzuki A, et al (1995) Melting relations of peridotite and the density crossover in planetary mantles. Chem Geol 120(3–4):207–221
O'Neill C, Jellinek A, Lenardic A (2007) Conditions for the onset of plate tectonics on terrestrial planets and moons. Earth Planet Sci Lett 261(1–2):20–32
Owen JE (2019) Atmospheric escape and the evolution of close-in exoplanets. Annu Rev Earth Planet Sci 47(1):67–90
Owen JE, Campos Estrada B (2020) Testing exoplanet evaporation with multitransiting systems. Mon Not R Astron Soc 491(4):5287–5297. https://doi.org/10.1093/mnras/stz3435
Owen JE, Schlichting HE (2024) Mapping out the parameter space for photoevaporation and core-powered mass-loss. Mon Not R Astron Soc 528(2):1615–1629
Owen JE, Wu Y (2013) Kepler planets: a tale of evaporation. Astrophys J 775(2):105. https://doi.org/10.1088/0004-637X/775/2/105
Owen JE, Wu Y (2017) The evaporation valley in the Kepler planets. Astrophys J 847(1):29. https://doi.org/10.3847/1538-4357/aa890a
Palme H, O'Neill HSC (2005) Cosmochemical estimates of mantle composition. In: Holland HD, Turekian KK (eds) Treatise on geochemistry, vol 2: The mantle and core. Elsevier–Pergamon, Oxford, pp 1–38
Palme H, Lodders K, Jones A (2014) 2.2 - Solar System abundances of the elements. In: Holland HD, Turekian KK (eds) Treatise on geochemistry, 2nd edn. Elsevier, Oxford, pp 15–36. https://doi.org/10.1016/B978-0-08-095975-7.00118-2
Parc L, Bouchy F, Venturini J, et al (2024) From super-Earths to sub-Neptunes: observational constraints and connections to theoretical models. Astron Astrophys 688:A59
Park RS, Jacobson RA, Gomez Casajus L, et al (2025) Io's tidal response precludes a shallow magma ocean. Nature 638(8049):69–73. https://doi.org/10.1038/s41586-024-08442-5
Parviainen H, Luque R, Palle E (2023) Spright: a probabilistic mass–density–radius relation for small planets. Mon Not R Astron Soc 527(3):5693–5716. https://doi.org/10.1093/mnras/stad3504
Patel JA, Brandeker A, Kitzmann D, et al (2024) JWST reveals the rapid and strong day-side variability of 55 Cancri e. Astron Astrophys 690:A159. https://doi.org/10.1051/0004-6361/202450748. arXiv:2407.12898 [astro-ph.EP]
Pepe F, Cristiani S, Rebolo R, et al (2021) ESPRESSO at VLT. On-sky performance and first results. Astron Astrophys 645:A96. https://doi.org/10.1051/0004-6361/202038306. arXiv:2010.00316 [astro-ph.IM]
Piaulet C, Benneke B, Rubenzahl RA, et al (2021) WASP-107b's density is even lower: a case study for the physics of planetary gas envelope accretion and orbital migration. Astron J 161(2):70. https://doi.org/10.3847/1538-3881/abcd3c
Piette AAA, Gao P, Brugman K, et al (2023) Rocky planet or water world? Observability of low-density lava world atmospheres. Astrophys J 954(1):29. https://doi.org/10.3847/1538-4357/acdef2. arXiv:2306.10100 [astro-ph.EP]
Plotnykov M, Valencia D (2020) Chemical fingerprints of formation in rocky super-Earths' data. Mon Not R Astron Soc 499(1):932–947. https://doi.org/10.1093/mnras/staa2615
Plotnykov M, Valencia D (2024) Observation uncertainty effects on the precision of interior planetary parameters. Mon Not R Astron Soc 530(3):3488–3499. https://doi.org/10.1093/mnras/stae993
Poirier JP (2003) Introduction to the physics of the Earth's interior, 2nd edn. Cambridge University Press, Cambridge
Putirka KD, Rarick JC (2019) The composition and mineralogy of rocky exoplanets: a survey of >4000 stars from the Hypatia Catalog. Am Mineral 104(6):817–829. https://doi.org/10.2138/am-2019-6787
Quanz SP, Ottiger M, Fontanet E, et al (2022) Large interferometer for exoplanets (LIFE): I. Improved exoplanet detection yield estimates for a large mid-infrared space-interferometer mission. Astron Astrophys 664:A21. https://doi.org/10.1051/0004-6361/202140366
Rathcke AD, Buchhave LA, de Wit J, et al (2025) Stellar contamination correction using back-to-back transits of TRAPPIST-1 b and c. Astrophys J 979(1):L19
Rauer H, Catala C, Aerts C, et al (2014) The PLATO 2.0 mission. Exp Astron 38(1–2):249–330. https://doi.org/10.1007/s10686-014-9383-4. arXiv:1310.0696 [astro-ph.EP]
Rauer H, Aerts C, Cabrera J, et al (2025) The PLATO mission. Exp Astron 59(3):26. https://doi.org/10.1007/s10686-025-09985-9

Reinhardt C, Meier T, Stadel JG, et al (2022) Forming iron-rich planets with giant impacts. Mon Not R Astron Soc 517(3):3132–3143. https://doi.org/10.1093/mnras/stac1853. arXiv:2204.04925 [astro-ph.EP]
Ricker GR, Winn JN, Vanderspek R, et al (2015) Transiting Exoplanet Survey Satellite (TESS). J Astron Telesc Instrum Syst 1:014003. https://doi.org/10.1117/1.JATIS.1.1.014003
Righter K, Ghiorso MS (2012) Redox systematics of a magma ocean with variable pressure-temperature gradients and composition. Proc Natl Acad Sci USA 109(30):11955–11960. https://doi.org/10.1073/pnas.1202754109
Rodríguez Martínez R, Gaudi BS, Schulze JG, et al (2023) A reanalysis of the composition of K2-106b: an ultra-short-period super-Mercury candidate. Astron J 165(3):97. https://doi.org/10.3847/1538-3881/acb04b. arXiv:2208.07883 [astro-ph.EP]
Rogers LA (2015) Most 1.6 Earth-radius planets are not rocky. Astrophys J 801(1):41. https://doi.org/10.1088/0004-637X/801/1/41
Rogers LA, Seager S (2010) A framework for quantifying the degeneracies of exoplanet interior compositions. Astrophys J 712:974–991. https://doi.org/10.1088/0004-637X/712/2/974
Rogers JG, Schlichting HE, Young ED (2024) Fleeting but not forgotten: the imprint of escaping hydrogen atmospheres on super-Earth interiors. Astrophys J 970(1):47
Rogers LK, Bonsor A, Le Bourdais É, et al (2025) Silicate mineralogy and bulk composition of exoplanetary material in polluted white dwarfs. Mon Not R Astron Soc 542(1):293–309. https://doi.org/10.1093/mnras/staf1221
Sakai T, Dekura H, Hirao N (2016) Experimental and theoretical thermal equations of state of MgSiO3 post-perovskite at multi-megabar pressures. Sci Rep 6(1):22652. https://doi.org/10.1038/srep22652
Santerne A, Brugger B, Armstrong DJ, et al (2018) An Earth-sized exoplanet with a Mercury-like composition. Nat Astron 2:393–400. https://doi.org/10.1038/s41550-018-0420-5. arXiv:1805.08405 [astro-ph.EP]
Santos NC, Adibekyan V, Mordasini C, et al (2015) Constraining planet structure from stellar chemistry: the cases of CoRoT-7, Kepler-10, and Kepler-93. Astron Astrophys 580:L13. https://doi.org/10.1051/0004-6361/201526850
Santos NC, Adibekyan V, Dorn C, et al (2017) Constraining planet structure and composition from stellar chemistry: trends in different stellar populations. Astron Astrophys 608:A94. https://doi.org/10.1051/0004-6361/201731359. arXiv:1711.00777
Saxena SK, Eriksson G (2015) Thermodynamics of iron at extreme pressures and temperatures. J Phys Chem Solids 84:70–74. https://doi.org/10.1016/j.jpcs.2015.03.006
Schulze JG, Wang J, Johnson JA, et al (2021) On the probability that a rocky planet's composition reflects its host star. Planet Sci J 2(3):113. https://doi.org/10.3847/PSJ/abcaa8. arXiv:2011.08893 [astro-ph.EP]
Seager S, Kuchner M, Hier-Majumder C, et al (2007) Mass-radius relationships for solid exoplanets. Astrophys J 669(2):1279–1297. https://doi.org/10.1086/521346
Seifahrt A, Stürmer J, Bean JL, et al (2018) MAROON-X: a radial velocity spectrograph for the Gemini observatory. In: Evans CJ, Simard L, Takami H (eds) Ground-based and airborne instrumentation for astronomy VII, p 107026D. https://doi.org/10.1117/12.2312936. arXiv:1805.09276
Shah O, Alibert Y, Helled R, et al (2021) Internal water storage capacity of terrestrial planets and the effect of hydration on the M - R relation. Astron Astrophys 646:A162. https://doi.org/10.1051/0004-6361/202038839
Si K, Karki B, Park J (2020) Deep mantle melting, global water circulation and its implications for the stability of the ocean mass. Prog Earth Planet Sci 7(1):76. https://doi.org/10.1186/s40645-020-00379-3
Sotin C, Grasset O, Mocquet A (2007) Mass–radius curve for extrasolar Earth-like planets and ocean planets. Icarus 191(1):337–351. https://doi.org/10.1016/j.icarus.2007.04.006
Spaargaren RJ, Ballmer MD, Bower DJ, et al (2020) The influence of bulk composition on the long-term interior-atmosphere evolution of terrestrial exoplanets. Astron Astrophys 643:A44. https://doi.org/10.1051/0004-6361/202037632
Spaargaren RJ, Wang HS, Mojzsis SJ, et al (2023) Plausible constraints on the range of bulk terrestrial exoplanet compositions in the solar neighborhood. Astrophys J 948(1):53. https://doi.org/10.3847/1538-4357/acac7d
Spaargaren RJ, Herbort O, Wang HS, et al (2025) Proto-planetary disk composition-dependent element volatility in the context of rocky planet formation. Astrophys J 703:A218. https://doi.org/10.1051/0004-6361/202556011
Spergel D, Gehrels N, Baltay C, et al (2015) Wide-Field InfrarRed Survey Telescope-Astrophysics Focused Telescope Assets. WFIRST-AFTA 2015 Report. https://doi.org/10.48550/arXiv.1503.03757. arXiv:1503.03757
Stähler SC, Khan A, Banerdt WB, et al (2021) Seismic detection of the Martian core. Science. https://doi.org/10.1126/science.abi7730

Stamenković V, Noack L, Breuer D, et al (2012) The influence of pressure-dependent viscosity on the thermal evolution of super-Earths. Astrophys J 748(1):41. https://doi.org/10.1088/0004-637X/748/1/41
Stixrude L (2014) Melting in super-Earths. Philos Trans R Soc A, Math Phys Eng Sci 372(2014):20130076. https://doi.org/10.1098/rsta.2013.0076
Stixrude L, Lithgow-Bertelloni C (2024) Thermodynamics of mantle minerals – III: the role of iron. Geophys J Int 237(3):1699–1733. https://doi.org/10.1093/gji/ggae126
Stock JW, Kitzmann D, Patzer ABC, et al (2018) Fastchem: a computer program for efficient complex chemical equilibrium calculations in the neutral/ionized gas phase with applications to stellar and planetary atmospheres. Mon Not R Astron Soc. https://doi.org/10.1093/mnras/sty1531
Suer TA, Jackson C, Grewal DS, et al (2023) The distribution of volatile elements during rocky planet formation. Front Earth Sci 11:1159412. https://doi.org/10.3389/feart.2023.1159412
Suissa G, Chen J, Kipping D (2018) A HARDCORE model for constraining an exoplanet's core size. Mon Not R Astron Soc 476(2):2613–2620. https://doi.org/10.1093/mnras/sty381. arXiv:1804.02019
Tackley PJ (1995) Mantle dynamics: influence of the transition zone. Rev Geophys 33(S1):275–282. https://doi.org/10.1029/95RG00291
Takahashi E (1986) Melting of a dry peridotite KLB-1 up to 14 GPa: implications on the origin of peridotitic upper mantle. J Geophys Res 91(B9):9367. https://doi.org/10.1029/JB091iB09p09367
Tange Y, Kuwayama Y, Irifune T, et al (2012) P - V - T equation of state of $MgSiO_3$ perovskite based on the MgO pressure scale: a comprehensive reference for mineralogy of the lower mantle. J Geophys Res, Solid Earth 117(B6):2011JB008988. https://doi.org/10.1029/2011JB008988. https://agupubs.onlinelibrary.wiley.com/doi/10.1029/2011JB008988
Tateno S, Hirose K, Ohishi Y, et al (2010) The structure of iron in Earth's inner core. Science 330(6002):359–361. https://doi.org/10.1126/science.1194662. arXiv:1409.5501.
Tayar J, Claytor ZR, Huber D, et al (2022) A guide to realistic uncertainties on the fundamental properties of solar-type exoplanet host stars. Astrophys J 927(1):31. https://doi.org/10.3847/1538-4357/ac4bbc
Taylor SR (2001) Solar System evolution: a new perspective, 2nd edn. Cambridge University Press, Cambridge. https://doi.org/10.1017/CBO9781139164368
Thiabaud A, Marboeuf U, Alibert Y, et al (2015) Elemental ratios in stars vs planets. Astron Astrophys 580:A30. https://doi.org/10.1051/0004-6361/201525963
Thomas SW, Madhusudhan N (2016) In hot water: effects of temperature-dependent interiors on the radii of water-rich super-Earths. Mon Not R Astron Soc 458(2):1330–1344. https://doi.org/10.1093/mnras/stw321
Timmermann A, Shan Y, Reiners A, et al (2023) Revisiting equilibrium condensation and rocky planet compositions: introducing the ECCOPLANETS code. Astron Astrophys 676:A52. https://doi.org/10.1051/0004-6361/202244850
Tinetti G, Drossart P, Eccleston P, et al (2016) The science of ARIEL (Atmospheric Remote-Sensing Infrared Exoplanet Large-Survey). In: MacEwen HA, Fazio GG, Lystrup M, et al (eds) Space telescopes and instrumentation 2016: optical, infrared, and millimeter wave. International Society for Optics and Photonics, vol 9904. SPIE, Bellingham, pp 658–667. https://doi.org/10.1117/12.2232370
Trierweiler IL, Doyle AE, Young ED (2023) A chondritic solar neighborhood. https://doi.org/10.48550/arXiv.2306.03743. arXiv:2306.03743
Tsuchiya T, Kawai K (2013) Ab initio mineralogical model of the Earth's lower mantle. In: Physics and chemistry of the deep Earth, pp 213–243
Turbet M, Bolmont E, Ehrenreich D, et al (2020) Revised mass-radius relationships for water-rich rocky planets more irradiated than the runaway greenhouse limit. Astron Astrophys 638:A41. https://doi.org/10.1051/0004-6361/201937151
Ulmer-Moll S, Santos NC, Figueira P, et al (2019) Beyond the exoplanet mass-radius relation. Astron Astrophys 630:A135. https://doi.org/10.1051/0004-6361/201936049
Umemoto K, Wentzcovitch RM (2011) Two-stage dissociation in MgSiO3 post-perovskite. Earth Planet Sci Lett 311(3):225–229. https://doi.org/10.1016/j.epsl.2011.09.032
Umemoto K, Wentzcovitch RM, Allen PB (2006) Dissociation of $MgSiO_3$ in the cores of gas giants and terrestrial exoplanets. Science 311(5763):983–986. https://doi.org/10.1126/science.1120865
Umemoto K, Wentzcovitch RM, Wu S, et al (2017) Phase transitions in MgSiO3 post-perovskite in super-Earth mantles. Earth Planet Sci Lett 478:40–45. https://doi.org/10.1016/j.epsl.2017.08.032. arXiv:1708.04767
Unterborn CT, Panero WR (2017) The effects of Mg/Si on the exoplanetary refractory oxygen budget. Astrophys J 845(1):61. https://doi.org/10.3847/1538-4357/aa7f79
Unterborn CT, Panero WR (2019) The pressure and temperature limits of likely rocky exoplanets. J Geophys Res Planets 124(7):1704–1716. https://doi.org/10.1029/2018JE005844
Unterborn CT, Dismukes EE, Panero WR (2016) Scaling the Earth: a sensitivity analysis of terrestrial exoplanetary interior models. Astrophys J 819(1):32. https://doi.org/10.3847/0004-637X/819/1/32

Unterborn CT, Desch SJ, Haldemann J, et al (2023) The nominal ranges of rocky planet masses, radii, surface gravities, and bulk densities. Astrophys J 944(1):42. https://doi.org/10.3847/1538-4357/acaa3b
Valencia D, O'Connell RJ, Sasselov D (2006) Internal structure of massive terrestrial planets. Icarus 181(2):545–554. https://doi.org/10.1016/j.icarus.2005.11.021
Valencia D, Sasselov DD, O'Connell RJ (2007) Detailed models of super-Earths: how well can we infer bulk properties? Astrophys J 665:1413–1420. https://doi.org/10.1086/519554
van den Berg AP, Yuen DA, Umemoto K, et al (2019) Mass-dependent dynamics of terrestrial exoplanets using ab initio mineral properties. Icarus 317:412–426. https://doi.org/10.1016/j.icarus.2018.08.016
Van Heck H, Tackley P (2011) Plate tectonics on super-Earths: equally or more likely than on Earth. Earth Planet Sci Lett 310(3–4):252–261
Vazan A, Sari R, Kessel R (2022) A new perspective on the interiors of ice-rich planets: ice–rock mixture instead of ice on top of rock. Astrophys J 926(2):150. https://doi.org/10.3847/1538-4357/ac458c
Vogt SS, Allen SL, Bigelow BC, et al (1994) HIRES: the high-resolution echelle spectrometer on the Keck 10-m Telescope. In: Crawford DL, Craine ER (eds) Instrumentation in astronomy VIII, p 362. https://doi.org/10.1117/12.176725
Wagner F, Sohl F, Hussmann H, et al (2011) Interior structure models of solid exoplanets using material laws in the infinite pressure limit. Icarus 214(2):366–376. https://doi.org/10.1016/j.icarus.2011.05.027
Wagner FW, Tosi N, Sohl F, et al (2012) Rocky super-Earth interiors. Structure and internal dynamics of CoRoT-7b and Kepler-10b. Astron Astrophys 541:A103. https://doi.org/10.1051/0004-6361/201118441
Wang HS, Lineweaver CH, Ireland TR (2018) The elemental abundances (with uncertainties) of the most Earth-like planet. Icarus 299:460–474. https://doi.org/10.1016/j.icarus.2017.08.024
Wang HS, Lineweaver CH, Ireland TR (2019a) The volatility trend of protosolar and terrestrial elemental abundances. Icarus 328:287–305. https://doi.org/10.1016/j.icarus.2019.03.018. arXiv:1810.12741 [astro-ph.EP]
Wang HS, Lineweaver CH, Ireland TR (2019b) The volatility trend of protosolar and terrestrial elemental abundances. Icarus 328:287–305. https://doi.org/10.1016/j.icarus.2019.03.018
Wang HS, Liu F, Ireland TR, et al (2019c) Enhanced constraints on the interior composition and structure of terrestrial exoplanets. Mon Not R Astron Soc 482(2):2222–2233. https://doi.org/10.1093/mnras/sty2749
Wang HS, Lineweaver CH, Quanz SP, et al (2022a) A model Earth-sized planet in the habitable zone of α Centauri A/B. Astrophys J 927:134. https://doi.org/10.3847/1538-4357/ac4e8c
Wang HS, Quanz SP, Yong D, et al (2022b) Detailed chemical compositions of planet-hosting stars: II. Exploration of the interiors of terrestrial-type exoplanets. Mon Not R Astron Soc. https://doi.org/10.1093/mnras/stac1119
Weeks A, Van Eylen V, Huber D, et al (2025) A link between rocky planet composition and stellar age. Mon Not R Astron Soc 539(1):405–421. https://doi.org/10.1093/mnras/staf474
Weidenschilling SJ (1978) Iron silicate fractionation and the origin of Mercury. Icarus 35:99–111. https://doi.org/10.1016/0019-1035(78)90064-7
Wicks JK, Singh S, Millot M, et al (2024) B1-B2 transition in shock-compressed MgO. Sci Adv 10(23):eadk0306. https://doi.org/10.1126/sciadv.adk0306
Wilson HF, Militzer B (2014) Interior phase transformations and mass–radius relationships of silicon–carbon planets. Astrophys J 793(1):34
Woitke P, Helling C, Hunter GH, et al (2018) Equilibrium chemistry down to 100 K: impact of silicates and phyllosilicates on the carbon to oxygen ratio. Astron Astrophys 614:A1. https://doi.org/10.1051/0004-6361/201732193
Wordsworth RD, Schaefer LK, Fischer RA (2018) Redox evolution via gravitational differentiation on low-mass planets: implications for abiotic oxygen, water loss, and habitability. Astron J 155:195. https://doi.org/10.3847/1538-3881/aab608
Wurm G, Trieloff M, Rauer H (2013) Photophoretic separation of metals and silicates: the formation of Mercury-like planets and metal depletion in chondrites. Astrophys J 769(1):78. https://doi.org/10.1088/0004-637X/769/1/78. arXiv:1305.0689 [astro-ph.EP]
Young ED, Shahar A, Schlichting HE (2023) Earth shaped by primordial H_2 atmospheres. Nature 616(7956):306–311. https://doi.org/10.1038/s41586-023-05823-0
Young ED, Stixrude L, Rogers JG, et al (2024) Phase equilibria of sub-Neptunes and super-Earths. Planet Sci J 5(12):268. https://doi.org/10.3847/PSJ/ad8c40
Yuan L, Steinle-Neumann G (2020) Strong sequestration of hydrogen into the Earth's core during planetary differentiation. Geophys Res Lett 47(15):e88303. https://doi.org/10.1029/2020GL088303
Zeng L, Seager S (2008) A computational tool to interpret the bulk composition of solid exoplanets based on mass and radius measurements. Publ Astron Soc Pac 120:983. https://doi.org/10.1086/591807

Zeng L, Sasselov D, Jacobsen S (2016) Mass-radius relation for rocky planets based on PREM. Astrophys J 819(2):127. https://doi.org/10.3847/0004-637X/819/2/127. arXiv:1512.08827
Zeng L, Jacobsen SB, Sasselov DD, et al (2019) Growth model interpretation of planet size distribution. Proc Natl Acad Sci USA 116(20):9723–9728. https://doi.org/10.1073/pnas.1812905116
Zeng L, Jacobsen SB, Hyung E, et al (2021) New perspectives on the exoplanet radius gap from a Mathematica tool and visualized water equation of state. Astrophys J 923(2):247. https://doi.org/10.3847/1538-4357/ac3137
Zhang M, Hu R, Inglis J, et al (2024) GJ 367b is a dark, hot, airless sub-Earth. Astrophys J Lett 961(2):L44. https://doi.org/10.3847/2041-8213/ad1a07. arXiv:2401.01400 [astro-ph]
Zhao Y, Ni D (2021) Machine learning techniques in studies of the interior structure of rocky exoplanets. Astron Astrophys 650:A177. https://doi.org/10.1051/0004-6361/202140375
Zieba S, Kreidberg L, Ducrot E, et al (2023) No thick carbon dioxide atmosphere on the rocky exoplanet TRAPPIST-1 c. Nature 620(7975):746–749
Zolotov MY (2011) On the chemistry of mantle and magmatic volatiles on Mercury. Icarus 212(1):24–41. https://doi.org/10.1016/j.icarus.2010.12.014